

MODEL-BASED ESTIMATION OF AMT VEHICLE CLUTCH KINETIC FRICTION
COEFFICIENT

By

Yu He

A THESIS

Submitted to
Michigan State University
in partial fulfillment of the requirements
for the degree of

Mechanical Engineering–Master of Science

2018

ABSTRACT

MODEL-BASED ESTIMATION OF AMT VEHICLE CLUTCH KINETIC FRICTION COEFFICIENT

By

Yu He

Driving performance and fuel economy are two important factors that attracts customers choosing certain type of vehicles. Those two factors can be improved largely by adopting optimized transmission gear-shifting strategy. The kinetic clutch friction coefficient is important to know to develop an optimized gear-shifting algorithm.

This thesis focus on estimating dynamic kinetic friction coefficient between two clutch plats of an automated manual transmission (AMT) vehicle when speed and temperature effects are involved. A Simulink model of an AMT vehicle was developed first, and a new friction coefficient estimation algorithm was then proposed and validated based on the developed Simulink model.

Several case studies are completed for the proposed estimation algorithm and fairly good simulation results are presented at the end of thesis.

ACKNOWLEDGEMENTS

I would like to take this opportunity to express my sincere appreciation to many individuals who have so graciously helped me during my MS study. I would like to thank Dr. Guoming (George) Zhu for being my advisor and supporting me during my MS program, and Drs. Zhaojian Li and Ranjan Mukherjee for serving my thesis committee. And I would also like to thank friends from our research group: Tianyi He, Chengsheng Miao and Donghao Hao who gave me advises regarding this vehicle model.

Lastly, I am overly grateful for my parents' continued support and warm-hearted solicitude that makes me full of courage to strive for the future.

TABLE OF CONTENTS

LIST OF TABLES	vi
LIST OF FIGURES	vii
KEY TO SYMBOL AND ABBREVIATIONS	iii
CHAPTER 1: INTRODUCTION	1
1.1 Motivation.....	1
1.2 Existing works.....	2
1.3 Vehicle Model Overview	2
1.4 Experiment Equipment/Software	5
CHAPTER 2: VEHICLE MODEL: PART ONE	6
2.1 Introduction	6
2.2 Driver Model.....	6
2.3 Shifting Threshold.....	7
2.4 Startup Logic	8
2.5 Shifting Logic.....	8
2.6 Actuator.....	10
2.7 Clutch parameters.....	11
CHAPTER 3: VEHICLE MODEL: PART TWO	13
3.1 Introduction	13
3.2 Driveline Physical Model.....	13
3.3 Transfer Function and State Model.....	17
3.3.1 Transfer Function and Continuous-Time State-Space Model	17
3.3.2 Discrete-Time State-Space Model.....	20
CHAPTER 4: INPUT TORQUE ESTIMATION	22
4.1 System Controllability and Observability	22
4.2 Prediction with a Feedforward Regulator	24
4.2.1 Deadbeat Design.....	24
4.2.2 Regular Pole Placement Design	26
4.2.3 LQR (Linear Quadratic Regulator) design	27
4.3 Integral Regulation Method (Discrete-Time).....	31
4.3.1 Integral Regulator Design.....	31

4.3.2 Deadbeat Design Comparison	35
CHAPTER 5: EFFECTS OF MODELING ERROR AND SOLUTIONS	40
5.1 Introduction	40
5.2 Modeling Error Due to Change of Vehicle Mass.....	40
5.3 Solutions to Handle the Vehicle Mass Modeling Error	41
5.4 Gradient Effect	42
CHAPTER 6: FRICTION COEFFICIENT CALCULATION.....	44
6.1 Calculation Method and Result.....	44
CHAPTER 7: CONCLUSION AND FUTURE WORK.....	47
7.1 Conclusion.....	47
7.2 Future Improvement.....	47
APPENDIX.....	48
REFERENCES	54

LIST OF TABLES

Table 1. Clutch parameters	12
Table 2. Gear ratios used.....	14
Table 3. Driveline system parameters	16

LIST OF FIGURES

Figure 1. Physical components of vehicle	3
Figure 2. Shifting algorithm for controlling clutch and engine speed	4
Figure 3. Overall thesis structure	5
Figure 4. Desired and actual vehicle speed responses	7
Figure 5. Simulated clutch pressure	9
Figure 6. Simulated gear state (0.5 represents the start-up period)	9
Figure 7. Clutch pressure during switching	11
Figure 8. Free Body Diagram of entire driveline system.....	16
Figure 9. Simulink state-space model interface	19
Figure 10. Simulink state-space model used to compare both system models.....	19
Figure 11. Comparison of physical and linear state-space model outputs.....	20
Figure 12. Simulated responses of both physical and discrete-time state-space model ..	22
Figure 13. Feedforward control method estimation.....	24
Figure 14. Input torques of physical system and state-space model with a deadbeat controller	26
Figure 15. Input torques of physical system and state-space model with a pole assignment of 0.5 and $-0.3 \pm 0.4j$	27
Figure 16. LQR estimated input and actual input torque.....	30
Figure 17. Block diagram of integral control estimation.....	33
Figure 18. Target system output (top) and state-space model output (bottom)	34
Figure 19. Integral control failed to track the physical system input when clutch state changes with closed-loop poles at ± 0.1 and ± 0.2	35
Figure 20. Estimation results for closed-loop poles at ± 0.5 and ± 0.8	36
Figure 21. Integral control of poles assigned at ± 0.01 and ± 0.02	37
Figure 22. Integral control of poles assigned at ± 0.001 and ± 0.002	37

Figure 23. Feedforward regulator (top) compare with integral regulator (bottom) between 66 and 66.2 second.....	39
Figure 24. Estimation of torque when modeling error exists.....	41
Figure 25. Torque estimation with real-time estimated vehicle mass.....	42
Figure 26. Detection algorithm flowchart.....	45
Figure 27. Error diminish within few time steps during slipping	45
Figure 28. Estimated friction coefficient	46
Figure 29. Driver model for acceleration and brake pedal inputs.....	49
Figure 30. Shifting threshold determination	50
Figure 31. Switch between start-up and driving modes and associated pressure	50
Figure 32. The Simulink gear-box model	51
Figure 33. Simulink driveline diagram without transmission.....	51
Figure 34. Torque loss calculation	52
Figure 35. Vehicle dynamic responses	52
Figure 36. Vehicle speed sensor.	52
Figure 37. Simulink system model overview	53

KEY TO SYMBOLS AND ABBREVIATIONS

AT	Automatic Transmission
A	Area (m ²)
MT	Manual Transmission
AMT	Automatic Manual Transmission
DCT	Dual Clutch Transmission
CVT	Continuously Variable Transmission
SISO	Single-Input-Single-Output
s	second
P	Pressure (Pa)
T	Torque (N*m)
<i>N</i>	Number of clutch surfaces
μ	Friction coefficient
μ_k	Kinetic friction coefficient
r_{eff}	Effective Radius
GR	Gear ratio
RPM	Revolution(s) per minute
T_{wind}	Power loss due to wind
T_{Road}	Power loss due to road slipping
T_{brake}	Power loss due to brake effect
$T_{gradient}$	Power loss due to grade effect
J_i	Inertia (kgm ²)
K	Torsional Spring constant (N*m/rad)

C Torsional Damping constant ($\text{N}\cdot\text{m}/(\text{rad}/\text{s})$)

θ Angle (rad)

CHAPTER 1: INTRODUCTION

1.1 Motivation

Due to the rising fossil fuel price and global climate change, vehicle manufacturers must improve vehicle fuel efficiency. Transmission is a key component. There are many types of transmission systems, that can be divided into five groups. They are automatic transmission (AT), manual transmission (MT), automatic manual transmission (AMT), dual clutch transmission (DCT) and continuously variable transmission (CVT). It is worth notice that the first four types of transmission systems use gear-shifting to achieve different gear ratio and clutch to break or transmit the power.

For AMT and DCT, a poorly designed transmission system can cause undesired vibration and discontinued power output during shifting, reducing passenger comfortableness. Discontinued power output also reduces the vehicle fuel economy due to unwanted engine idling; unwanted vibrations increases components fatigue and reduces vehicle life. Poor clutch engage timing may increase its slipping period, leading to power lost and also reducing the clutch life [1].

A good gear-shifting algorithm is necessary to achieve the desired vehicle performance. Engineers must understand the clutch friction dynamics very well to optimize the gear-shifting. The friction coefficient between two clutch plates is often viewed as a constant. This is true when the speed between two surfaces is low and temperature is constant. However, to improve vehicle fuel economy, passenger comfortableness, and vehicle life, the velocity and temperature effect to the friction coefficient must be considered. In this thesis, an algorithm will be proposed to estimate the clutch kinetic friction coefficient dynamically under driving condition.

1.2 Existing works

Research work in [2] has been done for dual-clutch transmission vehicles to improve vehicle fuel economy, where a three-parameter gear-shifting schedule, rather than the traditional two-parameters (engine and vehicle velocity, algorithm), is used. The third parameter is a compound parameter consisting of the road grade and the rolling resistance coefficient. With the three gear-shifting schedule, vehicle fuel economy can be improved by about 3%. This thesis adopts the three-parameter gear-shifting schedule for the vehicle model and seeks a method to estimate the friction coefficient between the two clutch plates during the gear-shifting.

An automatic manual transmission (AMT) vehicle model is built in 2014 MATLAB/Simulink. This model is constructed based on the previous dual-clutch transmission model and reference [2]. This model is used to validate the proposed estimation algorithm.

1.3 Vehicle Model Overview

For an AMT vehicle, the driver controls vehicle speed by pressing the acceleration or brake pedal, where the acceleration pedal determines engine throttle position that influences engine output torque. The engine output torque is transmitted via the clutch, gear box, driveline, and finally to wheels. On the other hand, the brake system adds negative torque to the driveline.

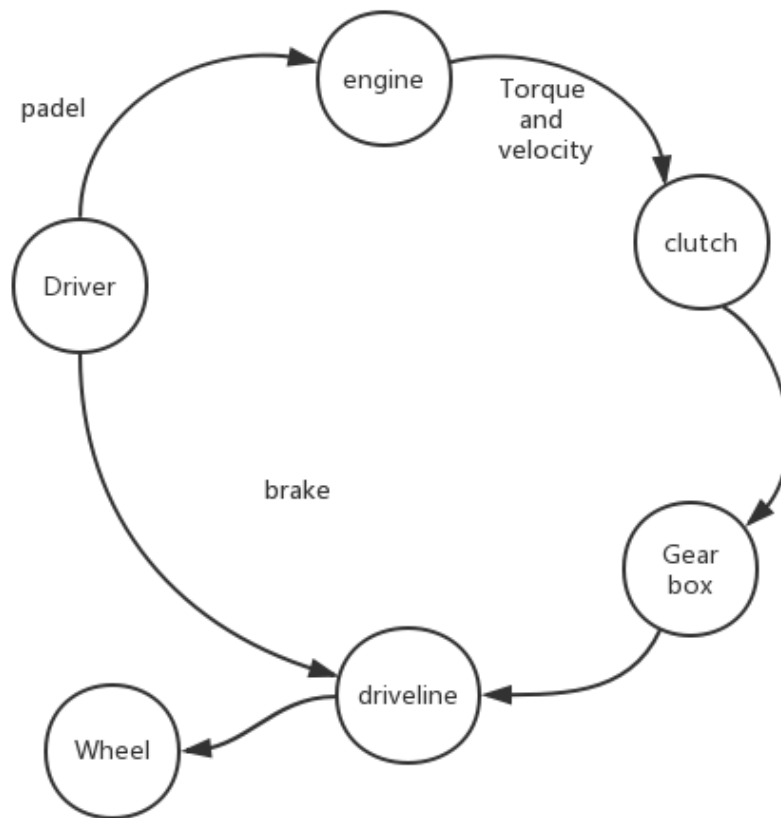


Figure 1. Physical components of vehicle

Figure 1 shows the vehicle driveline physical components. An AMT vehicle has its own gear-shifting strategy used to control the gear-shifting timing and clutch pressure based on acceleration (brake) pedal position, engine speed, and other available parameters. The gear-shifting strategy also controls the engine speed during the gear-shifting process.

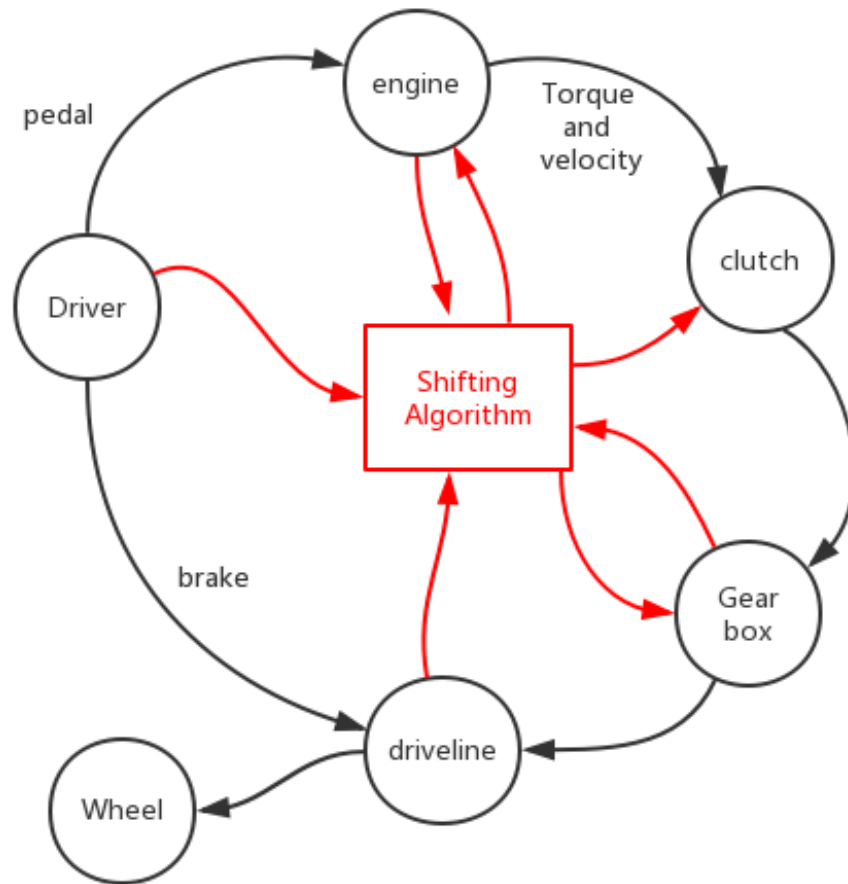


Figure 2. Shifting algorithm for controlling clutch and engine speed

The Simulink model is constructed based on the architecture shown in Figure 2. Because this thesis emphasizes on estimating the friction coefficient, simplifications are made to unrelated dynamics. For example, in practical application, the actuator controls clutch pressure in a closed-loop to reduce the error between desire and actual pressure. This model replaces the pressure actuator control system with a stable SISO (single-input-single-output) transfer function.

Since the main focus is on the clutch dynamics, vehicle wheel dynamics is simplified as well. Power transmitted through the driveline is converted to the vehicle acceleration based on Newton's law that consists vehicle mass, wheel inertia without considering wheel slipping dynamics, where slipping loss is simplified as kinetic friction between wheels and ground. The

friction coefficient of ground is set to a constant. Slipping loss could be define by magic tire formula in the future work.

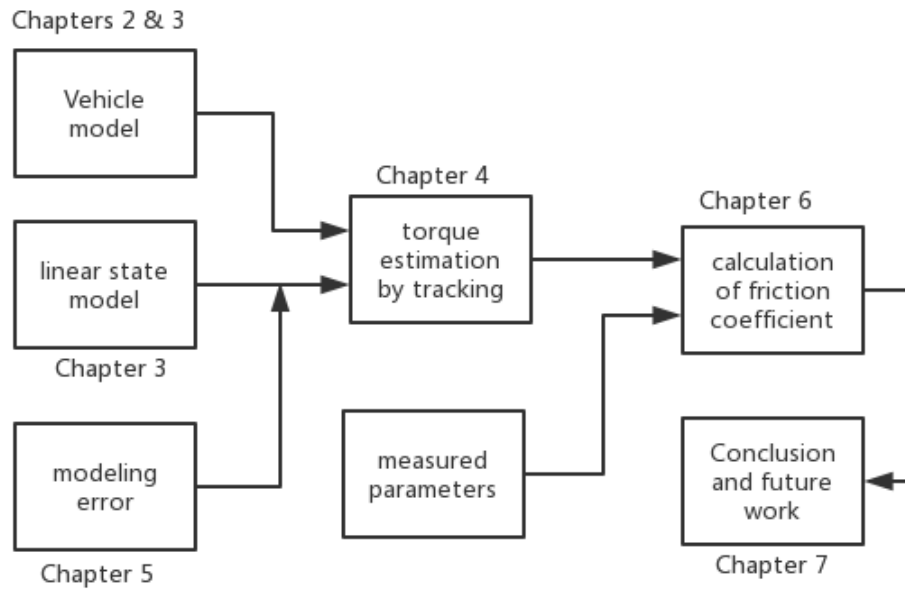


Figure 3. Overall thesis structure

1.4 Experiment Equipment/Software

This thesis focuses on developing a method of estimating clutch friction coefficient in real-time and validate the proposed method through simulation studies. All work is completed using a Windows 10 PC (personal computer) and the simulation model is constructed using 2014a MATLAB/Simulink.

CHAPTER 2: VEHICLE MODEL: PART ONE

2.1 Introduction

A Simulink model is developed to validate the proposed method. In this chapter, an AMT vehicle model will be introduced. This model contains a complete powertrain from engine to wheels, as well as a given desire vehicle speed profile describing driver behaviors. A driver model is also developed for the vehicle to match the desire speed profile by operating the acceleration and brake pedals. Gear-shifting strategy is also included.

2.2 Driver Model

The desire velocity profile is an $n \times 2$ matrix containing a time vector (the first column) between 0 and 174 second and a velocity vector (the second column) between from 0 to 90 km/h. During the simulation studies, vehicle starts at gear number one, gradually accelerates and switches gear up until the vehicle speed reaches about 90km/h, then, the vehicle slows down, and its gear shifts back down to one, and finally stops.

During the simulation study, another $n \times 2$ matrix (consisting of time and actual vehicle velocity) is generated. A PID controller (driver model) controls the vehicle speed to track the desired one. In another word, this controller behaviors like a driver to track the desired vehicle speed [3].

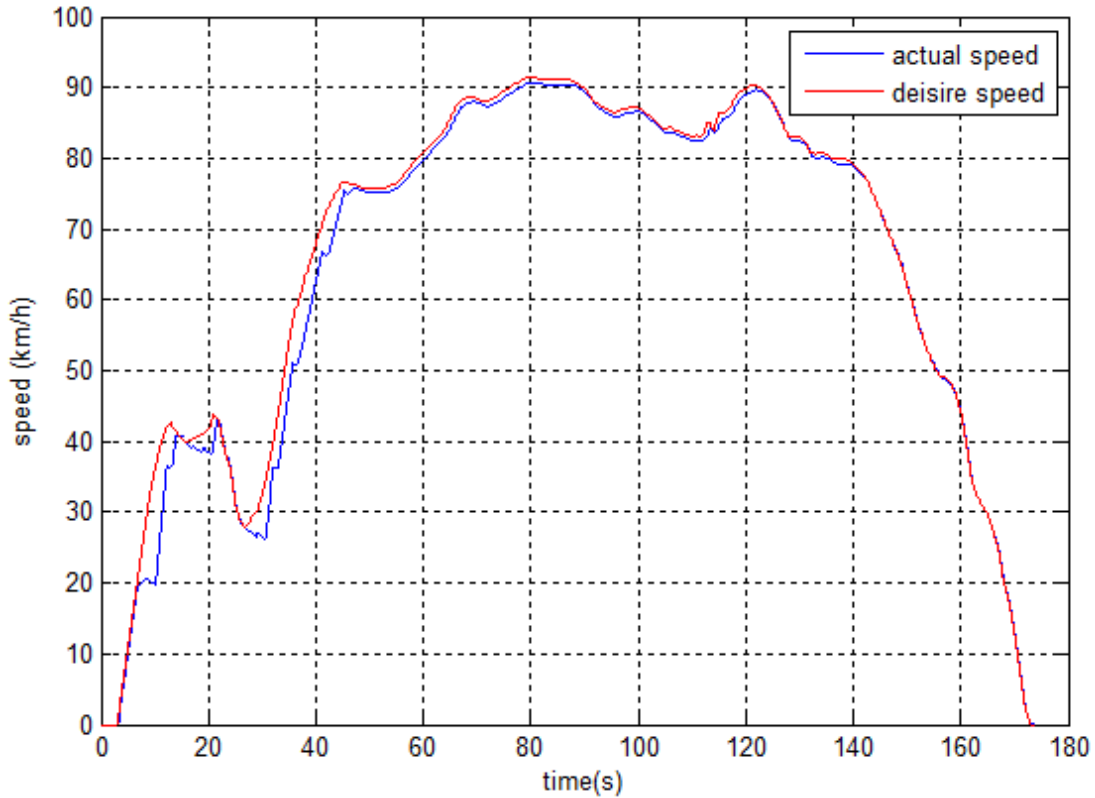


Figure 4. Desired and actual vehicle speed responses

The control input of this PID controller (the driver model) is also processed by two different saturation blocks. One limits the output between 0 and 1 and the saturated output is defined as the acceleration pedal signal, and the other limits the output between negative infinity and 0 and the associated saturated output is defined as the brake pedal input; see Figure 29 for a detailed Simulink block diagram in the Appendix.

2.3 Shifting Threshold

State flow chart in Simulink is used to dynamically determine the gear-shifting timing and threshold for each gear state. At each time step, the upshift and downshift thresholds are determined by two separated 2-D look up tables based on both pedal signals and current gear state. Meanwhile, the current vehicle speed is also compared with those two thresholds, once the engine speed exceeds one of those thresholds, the shifting logic will be activated; see Figure

30 in the Appendix for a detailed Simulink gear-shifting threshold determination logic.

2.4 Startup Logic

When the engine speed is below 800 RPM, the startup logic will be activated. In this case, the clutch pressure is calculated by the following formula

$$P = T \frac{1}{N * r_{eff} * \mu * A} \quad (1)$$

where T is the demanding torque, N is the number of clutch pack, r_{eff} is effective clutch radius, A is effective clutch area and μ is the kinetic friction coefficient of clutch; see reference [4] for details.

After the engine speed rises above 850 RPM, the startup logic ends and driving logic is used; see Figure 31 in the Appendix for the Simulink block diagram about start-up pressure and switches between start-up and driving modes.

2.5 Shifting Logic

When the shifting threshold is met, the clutch plates first disengages from each other. After the clutch is fully disengaged, the gear state increases or decreases depending on which gear-shifting threshold is met. Next, a pre-shifting pressure P_{pre} is applied to the clutch plates to allow clutch plate contacting and slipping, which helps reducing the speed difference between clutch plates and preventing driveline vibrations caused by sudden lock-up. The pre-shifting pressure is a function of the desire torque, speed difference between clutch plates and other clutch parameters [5].

$$P_{pre} = f(T, N, r_{eff}, \mu, A, v_{diff}) \quad (2)$$

After the speed difference is reduced below 50 RPM, full clutch pressure will be applied, and the clutch will be locked-up. This is the complete gear-shifting logic used in this model; see

Figure 5 and Figure 6 for simulation results.

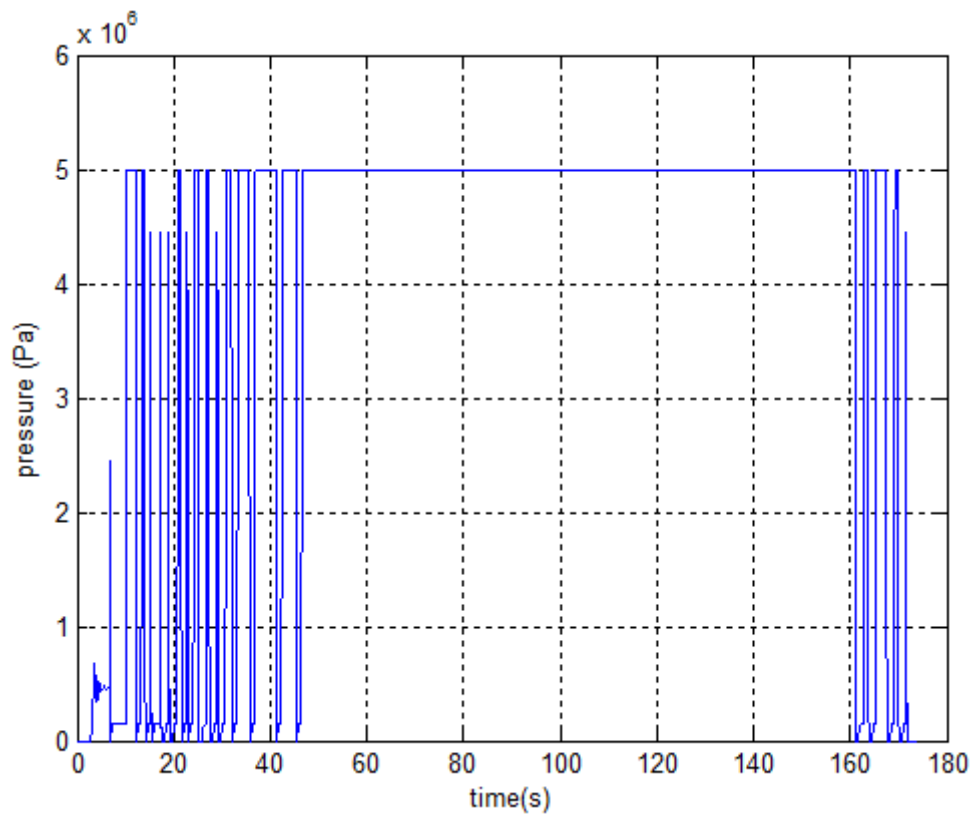


Figure 5. Simulated clutch pressure

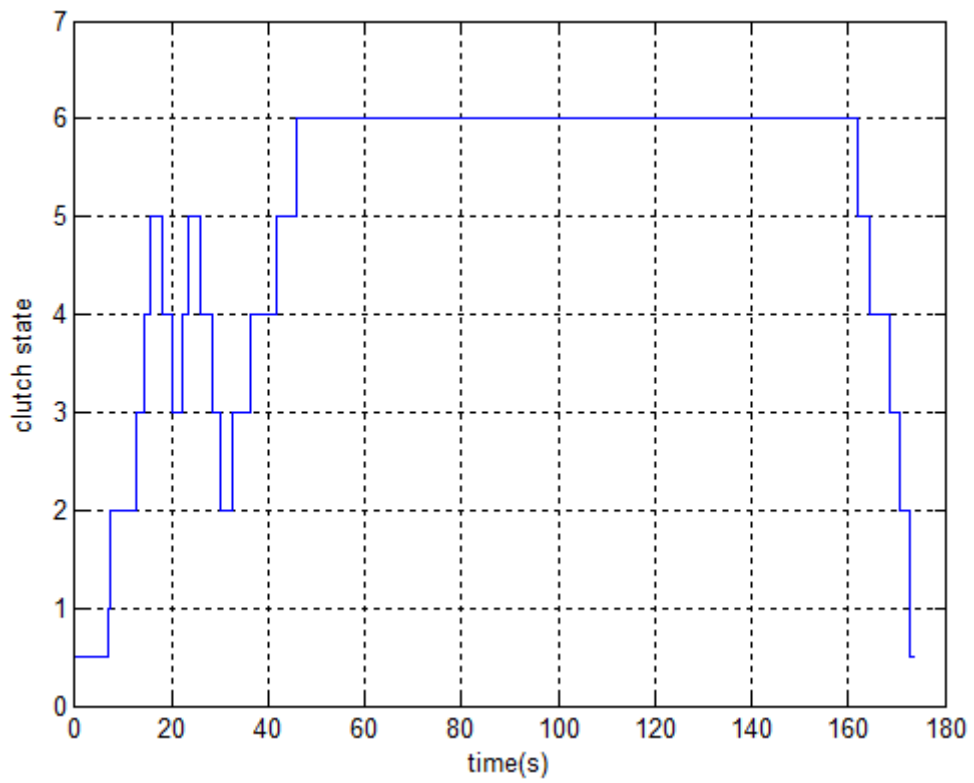


Figure 6. Simulated gear state (0.5 represents the start-up period)

2.6 Actuator

There are two methods that can be used to calculate the desired clutch pressure: startup and driving pressure. Note that the startup pressure can be calculated using equation (1) and this subsection mainly addresses the driving pressure calculation. Constant C1 is defined to represent the state of clutch. When clutches need to be engaged, C1 is set to 1, and otherwise, it is set to 0. Then, C1 is inputted to a ramp function, and the output of the ramp function is treated as the clutch actuator input.

A switching function is used to determine if the startup or driving pressure is used as the input to the clutch actuator. The actuator is simplified as a second order transfer function

$$H(s) = \frac{1}{0.02s + 1} \quad (3)$$

The Simulink diagram of the model can be found in Figure 31 in Appendix. The final pressure applied on clutch plates during a single gear-shifting period is shown in the figure below.

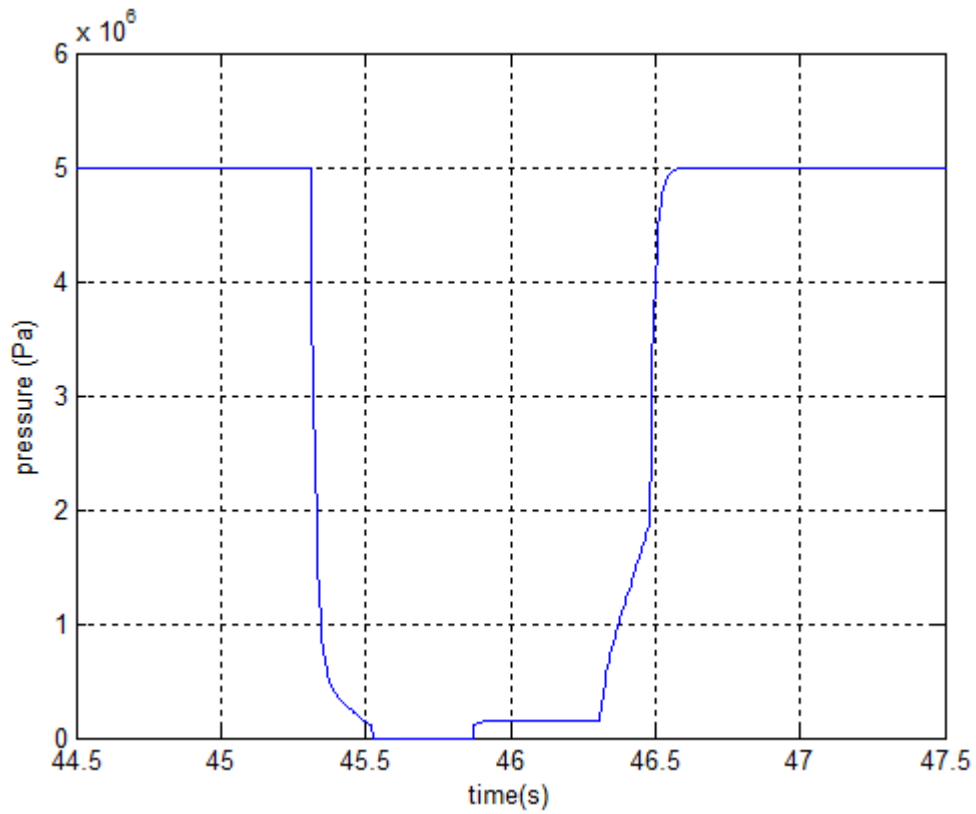


Figure 7. Clutch pressure during switching

2.7 Clutch parameters

In this model, a Simscape clutch block is used. The input of the Simscape clutch model is connected to the engine output and the output is connected to the gear box. The clutch model parameters are given below in Table 1.

Table 1. Clutch parameters

Effective torque radius	130	mm
Number of friction surfaces:	4	
Engagement piston area:	0.001	m^2
Kinetic friction coefficient:	0.3	
Static friction coefficient:	0.31	
De-rating factor	1	
Clutch velocity tolerance	0.001	rad/s
engagement threshold pressure	1	P_a

CHAPTER 3: VEHICLE MODEL: PART TWO

3.1 Introduction

In this chapter, the driveline model from clutch output to the vehicle wheels will be discussed. There are two inputs to the driveline system: torque input from the clutch output shaft and torque loss due to braking and tire slipping. The driveline system consists of a gear box for gear-ratio change, a set of gears determining the vehicle final ratio, and the drive shaft transmitting torque.

The driveline system is divided into two parts connected by spring and damper dynamics used to model a flexible driving shaft; see Figure 8. Multiple spring and damper dynamics can be used to model the driveline system with increased degree of freedoms. Increased degree of freedoms improves the model accuracy, but it also increases the system model complexity.

After the physical driveline model is defined, one can transform the system into a state-space model by choosing proper states. Assuming the loss of torque can be predicted, the system can be reduced down to three states of an SISO (single-input-single-output) system. In this Chapter, the Simscape physical model of driveline system and Simulink state-space model will be presented with detailed derivation. During the simulation studies, it is assumed that the vehicle speed can be directly measured, and the vehicle mass is constant. All the gears ratios and inertias of driveline components are predetermined or assumed to be known. The goal is to determine the clutch torque output with known vehicle speed.

3.2 Driveline Physical Model

As shown in Figure 32 of Appendix section, torque input T_{in} (input 1 in the Simulink diagram) is applied through the variable ratio transmission to the output shaft. The gear ratio of the variable ratio transmission is determined by the acceleration pedal position, engine speed and the third parameter (see [2] for details). Each time the gear shifts, the clutch will be fully

dis-engaged with zero input torque to the driveline, the engine speed is changed to match the driveline speed for the next gear-ratio, and the clutch will be re-engaged.

This gear box consists of six gears, the gear ratios are measured from an existing vehicle and are shown below:

Table 2. Gear ratios used

Gear	Gear Ratio
1	3.78
2	2.18
3	1.43
4	1.03
5	0.935
6	0.84

Note that the torque transmitted by the variable ratio transmission can be determined by

$$T_{transmitted} = T_{input} \times Gear\ ratio \quad (4)$$

and the linear velocity relationship is defined by

$$V_{transmitted} = \frac{V_{input}}{Gear\ Ratio} \quad (5)$$

Therefore, at high gear ratio, the output torque is reduced with high speed [6]; at low gear ratio, the output torque is increased with slow speed, satisfying the traditional convention.

Figure 33 in the Appendix shows the rest of the driveline system, where final ratio is a fixed at 3.7. The transmission ratio R_d of the entire driveline is given by:

$$R_d = Gear\ ratio \times final\ ratio \quad (6)$$

Subsystem 1 in Figure 33 represents the spring and damper dynamics used to describe the shaft vibration dynamics. Assuming that the road effect (friction coefficient) and brake/friction

torque is known, the torque loss can be calculated in the Simulink block shown in Figure 34 in the Appendix.

The three major factors causing torque loss are aero-dynamics, braking and slipping between road and tires. Knowing the vehicle velocity, the aero dynamic torque loss can be calculated by the following formula

$$T_{wind} = \left(\frac{V_{vehicle}}{3.6}\right)^2 \times \frac{A_v \times C_d \times \rho}{2} \times R \quad (7)$$

where A_v is the front vehicle area, C_d is the aerodynamic drag coefficient, ρ is the air density and R is the tire radius. In this formula, constant 3.6 converts $V_{vehicle}$ from km/h to m/s.

The road slipping loss is simplified by the following formula

$$T_{Road} = Mass \times \mu_{road} \times g \times R \quad (8)$$

where mass is the total vehicle mass, μ_{road} is the kinetic friction coefficient between road and tires, and g is the gravitational constant (9.81 at sea level).

When vehicle is faster than the desire speed, driver usually uses brake to reduce vehicle speed. Note that the driver model used is a PID controller. The brake loss is associated with the output of the driver PID controller; see driver model section for details.

The total torque loss is defined by

$$T_{loss} = T_{brake} + T_{Road} + T_{wind} \quad (9)$$

The road gradient effect is not counted in this formula by assuming that it is operated on a leveled road. If gradient is changing, the following road gradient term needs to be added to equation (9)

$$T_{gradient} = Mass \times \sin\theta \times g \times \left(\frac{V_{vehicle}}{3.6}\right) \quad (10)$$

where θ in equation (10) is the slope of road. The total loss of torque becomes [7]

$$T_{loss} = T_{brake} + T_{Road} + T_{wind} + T_{gradient} \quad (11)$$

After T_{loss} is determined, the response of driveline system can be found using the

Simulink diagram defined in Figure 35 in the Appendix.

Figure 35 in the Appendix shows that the input torque minus the torque loss applies to the total vehicle inertia to generate vehicle speed and the simulation is completed in continuous-time domain. The AMT control algorithm and driver model alter input torque and clutch state dynamically to accomplish this simulation [8].

Now, with all the driveline components connected, the driveline system model architecture is shown below [9].

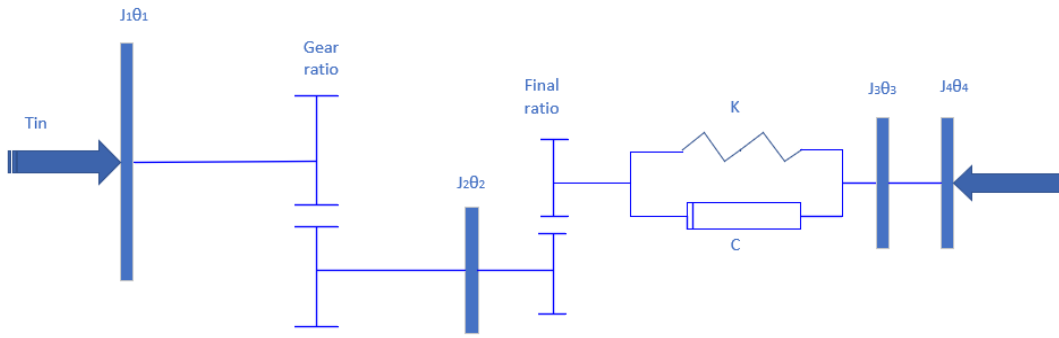


Figure 8. Free Body Diagram of entire driveline system

Based on Figure 8, two equations can be derived to describe the system dynamics.

$$\begin{aligned}
 (J_1 \times GR^2 + J_2)\ddot{\theta}_2 &= T_{in} \times GR - \left(\frac{\theta_2}{final\ ratio} - \theta_3\right) \frac{k}{final\ ratio} \\
 &\quad - \left(\frac{\dot{\theta}_2}{final\ ratio} - \dot{\theta}_3\right) \frac{c}{final\ ratio} \tag{12} \\
 (J_3 + J_4)\ddot{\theta}_4 &= \left(\frac{\theta_2}{final\ ratio} - \theta_3\right) k + \left(\frac{\dot{\theta}_2}{final\ ratio} - \dot{\theta}_3\right) c - T_{los}
 \end{aligned}$$

All parameters in above equations are given in the following table.

Table 3. Driveline system parameters

J_1	0.01	kgm ²
-------	------	------------------

J_2	0.02	kgm ²
J_3	0.01	kgm ²
J_4	157.7504	kgm ²
K	1500	N*m/rad
C	20	N*m/(rad/s)

With above equations and parameters defined, now we are ready to derive the transfer function and state-space model.

3.3 Transfer Function and State Model

3.3.1 Transfer Function and Continuous-Time State-Space Model

Reference [10] presents a state-space model below, where

$$\begin{aligned}
x_1 &= \dot{\theta}_2 \\
x_2 &= \dot{\theta}_4 \\
x_3 &= \theta_2 - 3.7\theta_3 \\
u_1 &= T_{in} \times GR \\
u_2 &= T_{loss}
\end{aligned} \tag{13}$$

It is worth notice that J_1 (the inner shaft inertia) is very small, comparing with the total vehicle inertia. Hence, the system model can be simplified by assuming $J_1 = J_1 \times GR^2$, which results in a linear system model with a state-space model in the form of [11]. A comparison between the original nonlinear and simplified linear models will be conducted at the end of this subsection. The linear state-space system model is shown below [12].

$$\begin{aligned}
0.03\dot{x}_1 &= u_1 - x_3 \times \frac{1500}{3.7^2} - \frac{(x_1 - 3.7x_2)20}{3.7^2} \\
157.76\dot{x}_2 &= \frac{x_3}{3.7} \times 1500 + \left(\frac{x_1}{3.7} - x_2\right) 20 - u_2 \\
\dot{x}_3 &= x_1 - 3.7x_2
\end{aligned} \tag{14}$$

$$y = x_2$$

Reorganize the above state-space equations, the linear state-space model is given below

[13]:

$$\begin{bmatrix} \dot{x}_1 \\ \dot{x}_2 \\ \dot{x}_3 \end{bmatrix} = \begin{bmatrix} \frac{20}{0.03 \times 3.7^2} & \frac{74}{0.03 \times 3.7^2} & -\frac{1500}{0.03 \times 3.7^2} \\ \frac{20}{3.7 \times 157.76} & -\frac{20}{157.76} & \frac{1500}{3.7 \times 157.76} \\ 1 & -3.7 & 0 \end{bmatrix} \begin{bmatrix} x_1 \\ x_2 \\ x_3 \end{bmatrix} \quad (15)$$

$$+ \begin{bmatrix} \frac{1}{0.03} & 0 \\ 0 & -\frac{1}{157.76} \\ 0 & 0 \end{bmatrix} \begin{bmatrix} u_1 \\ u_2 \end{bmatrix}$$

$$y = [0 \quad 1 \quad 0] \begin{bmatrix} x_1 \\ x_2 \\ x_3 \end{bmatrix} \quad (16)$$

The state-space model coefficient matrices A , B , C , and D are therefore

$$A = \begin{bmatrix} \frac{20}{0.03 \times 3.7^2} & \frac{74}{0.03 \times 3.7^2} & -\frac{1500}{0.03 \times 3.7^2} \\ \frac{20}{3.7 \times 157.76} & -\frac{20}{157.76} & \frac{1500}{3.7 \times 157.76} \\ 1 & -3.7 & 0 \end{bmatrix} \quad (17)$$

$$B = \begin{bmatrix} \frac{1}{0.03} & 0 \\ 0 & -\frac{1}{157.76} \\ 0 & 0 \end{bmatrix} \quad (18)$$

$$C = [0 \quad 1 \quad 0] \quad (19)$$

and

$$D = [0 \quad 0] \quad (20)$$

Now, these matrix values are entered to Simulink continuous-time transfer function block to form the physical system model; see Figure 9 and Figure 10.

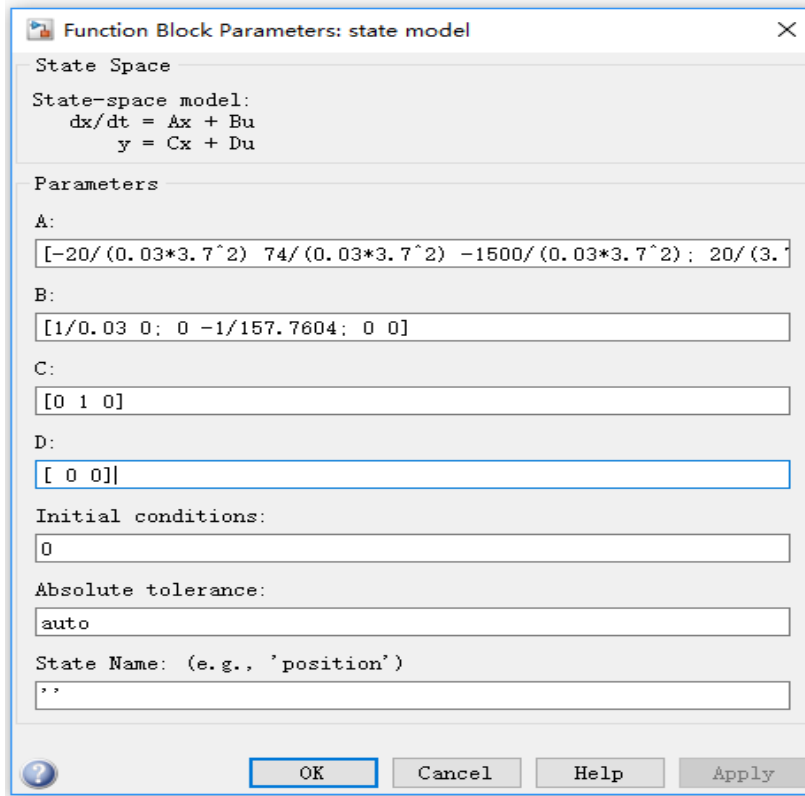


Figure 9. Simulink state-space model interface

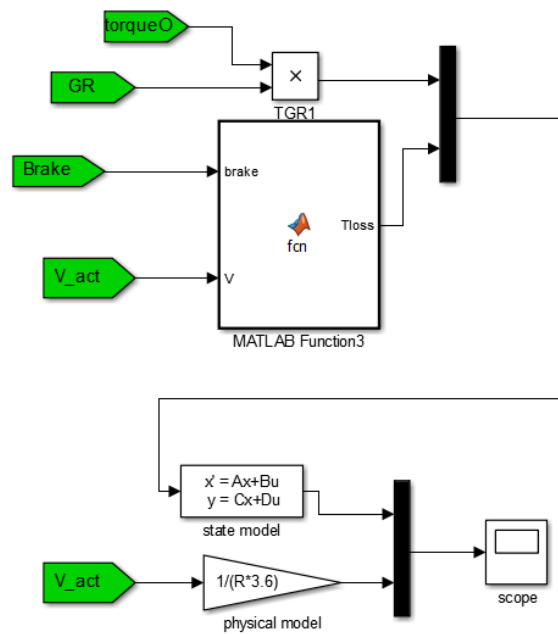


Figure 10. Simulink state-space model used to compare both system models

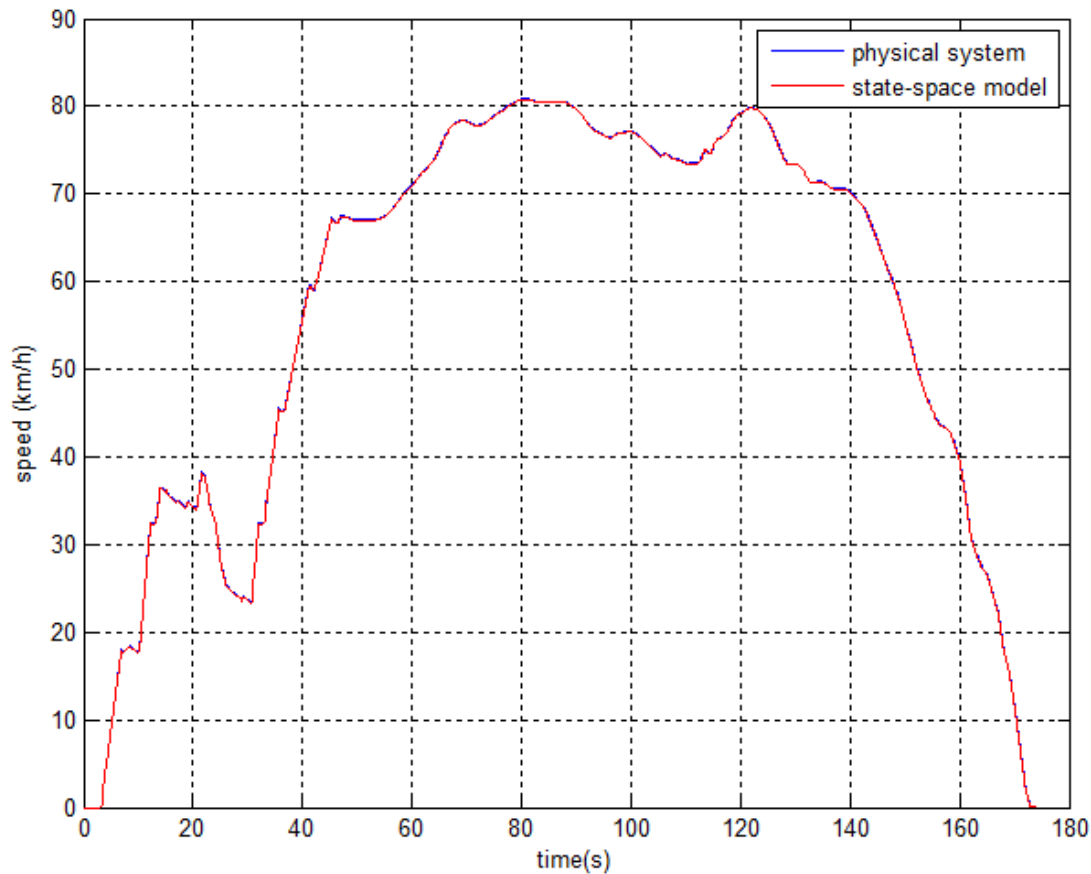


Figure 11. Comparison of physical and linear state-space model outputs

The simulated outputs of the physical nonlinear and linear state-space models are very close (blue and red lines are almost overlapped together in Figure 11), indicating that the linear state-space model can be used to represent the physical nonlinear system. The rest of research in this thesis will be based on the linear state-space model.

3.3.2 Discrete-Time State-Space Model

One of the way to estimate the driveline system input from its output is to design a set point regulator for the driveline state-space model. By regulating the output of state-space model to its physical model output, the input of the state-space model will track the physical model input.

To make the set point regulator converge to the desire target as quick as possible, and reduce the calculation load, the system is discretized based on the continuous-time model. By

placing the closed-loop poles of the discrete-time tracking system at or near the origin of the complex plane, the dead-beat design can be achieved, and hence, the system response will converge to the desire target in a few time steps [14].

To convert the following continuous-time system

$$\dot{x}(t) = Ax(t) + Bu(t) \quad (21)$$

$$y(t) = Cx(t) \quad (22)$$

into a discrete-time system below

$$x(k + 1) = Gx(k) + Hu(k) \quad (23)$$

$$y(k) = Cx(k) \quad (24)$$

The following formulas are used:

$$G = e^{AT} \quad (25)$$

$$H = \int_0^T e^{A(T-\tau)} B d\tau \quad (26)$$

where A , B and C are continuous-time state-space model matrices and T is the sample period, where T is selected to be 0.005 second. With the given $T = 0.005$ s, matrices G and H are calculated using the following MATLAB commands

$$G = \text{expm}(A \times T) \quad (27)$$

$$\text{fun} = @(x) \text{expm}(A \times x); \quad (28)$$

$$H = \text{integral}(\text{fun}, 0, T, 'ArrayValued', true) \times B \quad (29)$$

Resulting in

$$G = \begin{bmatrix} 0.745394 & 0.942042 & -15.957481 \\ 0.000179 & 0.999337 & 0.011228 \\ 0.004369 & -0.016166 & 0.958052 \end{bmatrix} \quad (30)$$

$$H = \begin{bmatrix} 0.145693 & -0.000015 \\ 0.000015 & -0.000032 \\ 0.000382 & 0.00000027 \end{bmatrix} \quad (31)$$

Now conduct the simulation studies for both physical nonlinear and discrete-time state-space models using the same input as physical model; see Figure 12 for simulation results.

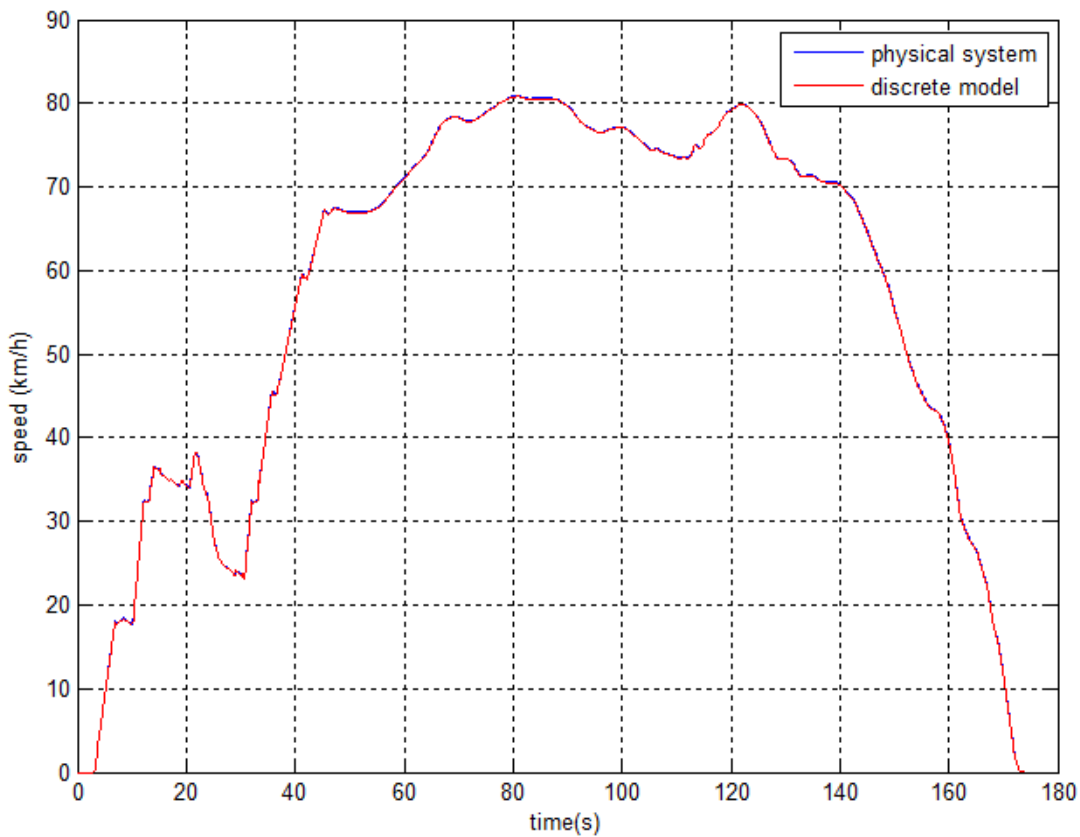


Figure 12. Simulated responses of both physical and discrete-time state-space model

It can be seen that the discrete-time system model describes the physical model accurately and the control design in the remaining thesis will be based on the discrete-time system model.

CHAPTER 4: INPUT TORQUE ESTIMATION

4.1 System Controllability and Observability

Since the goal is to design a controller to regulate the state-space model output to the

physical model output, it is good to investigate important system properties before controller design [15].

The original system has two inputs and one output, and in theory, it is impossible to estimate both inputs from the given output. However, since the torque loss can be estimated using (10) or (11), and the torque loss T_{loss} can be assumed to be known input and the system is reduced down to an SISO (single input single output) system. In this case, H in equation (31) is therefore reduced to

$$H = \begin{bmatrix} 0.145693 \\ 0.000015 \\ 0.000382 \end{bmatrix} \quad (32)$$

With this H , the system controllability and observability can be investigated. Note that the controllability matrix is defined by

$$C = [H, GH, G^2H] \quad (33)$$

resulting in the following full rank matrix

$$C = \begin{bmatrix} 0.145693 & 0.102519 & 0.060468 \\ 0.000015 & 0.000045 & 0.000075 \\ 0.000382 & 0.001002 & 0.001407 \end{bmatrix} \quad (34)$$

and therefore, the system is controllable. Similarly, the observability matrix is defined below.

$$O = \begin{bmatrix} C \\ CG \\ CG^2 \end{bmatrix} \quad (35)$$

yielding the following full rank matrix

$$O = \begin{bmatrix} 0 & 1 & 0 \\ 0.000179 & 0.999337 & 0.011228 \\ 0.000362 & 0.998662 & 0.019118 \end{bmatrix} \quad (36)$$

and as a result, the system is also observable.

4.2 Prediction with a Feedforward Regulator

4.2.1 Deadbeat Design

Now it is time to predict the input torque from the output speed. A set point regulator will be designed to steer the discrete-time system output to its physical system output. In this case, the discrete-time system input will converge to actual one.

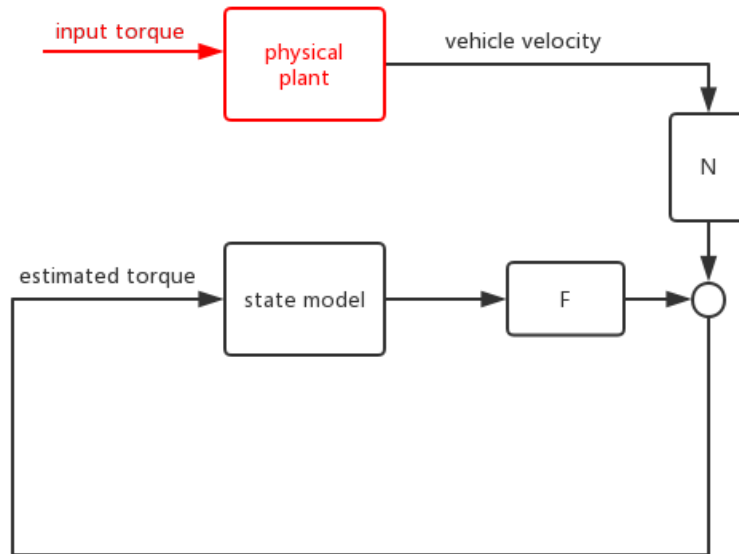


Figure 13. Feedforward control method estimation

As shown in Figure 13 the discrete time system input will be designed in the following form

$$u(k) = Fx(k) + v \quad (37)$$

where vector F will be designed such that poles of $G + HF$ are within the unit circle. To achieve fast converge, it is desired to assign all the poles at origin of the complex plane. However, the multiplicity of poles cannot exceed the rank of matrix H . Therefore, the poles are placed at $-0.1, 0, 0.1$. Using MATLAB pole placement command, the associated vector F is

$$F = [-10.56578 \quad -1.04963 \times 10^5 \quad 1.00957 \times 10^3] \quad (38)$$

and the associated closed-loop system is

$$x(k + 1) = (G + HF)x(k) + Hv(k) \quad (39)$$

$$y(k) = Cx(k) \quad (40)$$

The transfer function from v to y is

$$C[zI - (G + HF)]^{-1}H \quad (41)$$

At steady-state, the transfer function becomes

$$-C[(G + HF)]^{-1}H \quad (42)$$

Let N be

$$N = -[C(G + HF)^{-1}H]^{-1} \quad (43)$$

Note that when $v = Nr$, the steady-state system output is

$$y_{ss} = r \quad (44)$$

In this case, r is the physical system output and N is calculated using (43) to be

$$N = 1.050022 \times 10^5 \quad (45)$$

Since feedforward control requires all the states, identity matrix is used for C as below

$$C = \begin{bmatrix} 1 & 0 & 0 \\ 0 & 1 & 0 \\ 0 & 0 & 1 \end{bmatrix} \quad (46)$$

Note that in case that not all states are available, Kalman state estimator could be used to estimate the state vector. The simulation results of the set point regulator is given in Figure 14 below.

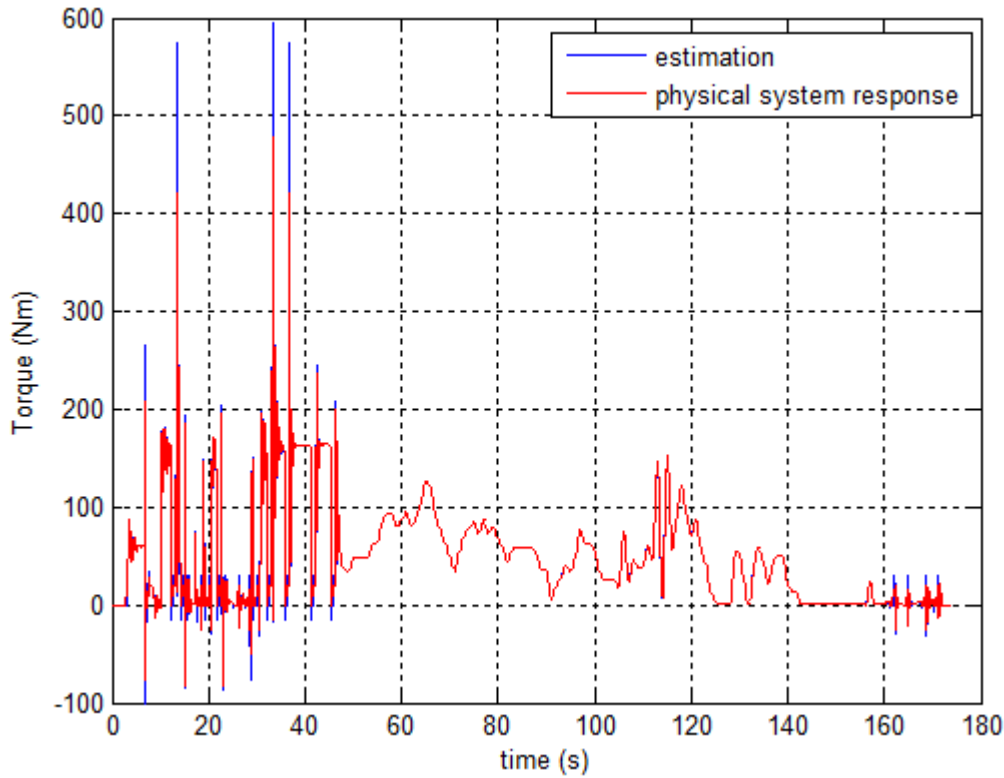


Figure 14. Input torques of physical system and state-space model with a deadbeat controller

Figure 14 shows that the estimated input to the state-space model converges to the physical system input quickly. In next section, the controllers assigned to other pole locations will be investigated to see if the convergence can be improved.

4.2.2 Regular Pole Placement Design

To compare the influence of different methods and different pole locations to the estimation performance. Conventional pole placement method will be used, and poles will not be assigned very close to the origin of the complex plane.

Three poles of matrix $G + HF$ will be assigned to 0.5, $-0.3+0.4j$ and $-0.3-0.4j$ so that each pole has distance of 0.5 from the origin. Since all the poles are within the unit circle, the estimated input torque is expected to converge to the actual torque but slower than the deadbeat design.

By using place command in MATLAB, the resulting vector F is

$$F = [-10.522922 \quad -9.806918 \times 10^4 \quad 4.649292 \times 10^2] \quad (47)$$

And using the following formula for N

$$N = -[C(G + HF)^{-1}H]^{-1} \quad (48)$$

leading to

$$N = 9.810812 \times 10^4 \quad (49)$$

With such newly designed F and N , the simulation results are shown in Figure 15. The estimated input converges to the correct value as well. The effect of this design to estimation robustness and stability will be discussed later.

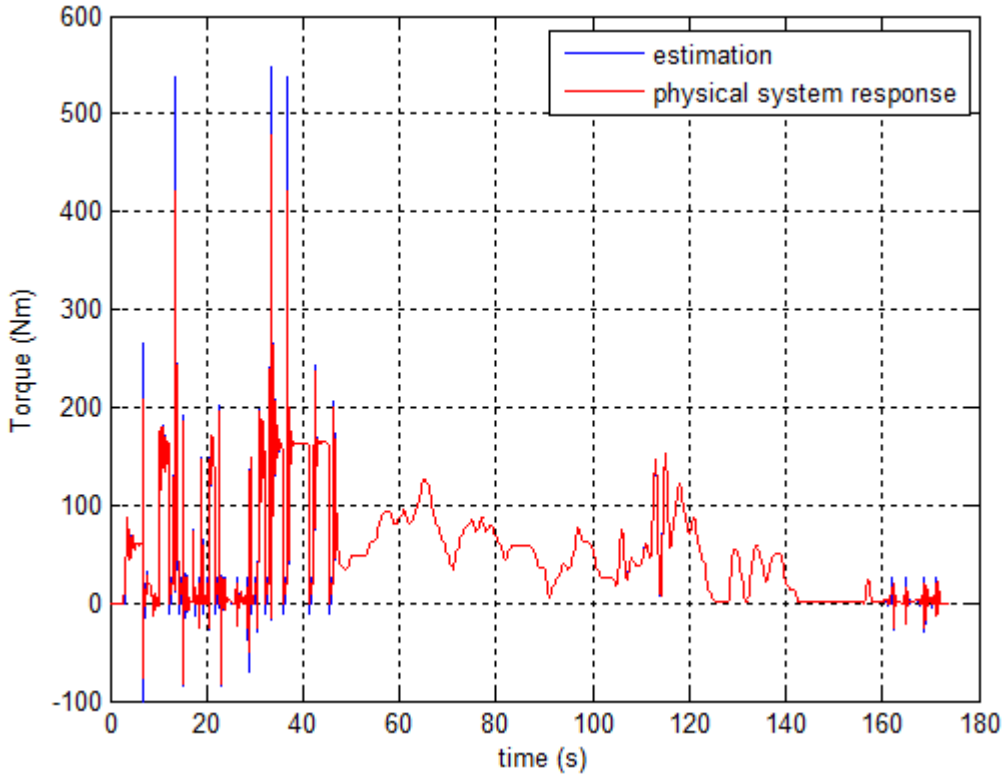


Figure 15. Input torques of physical system and state-space model with a pole assignment of 0.5 and $-0.3 \pm 0.4j$.

4.2.3 LQR (Linear Quadratic Regulator) design

LQR design is an optimal control design method. In the regular feedforward controller, the designed vector F for the system input

$$u = Fx \quad (50)$$

is a tradeoff between transient response performance and control effort. This means that for the high gain F , the input u could be extremely large with fast convergence, and for the low gain F , u would be relatively small with slow convergence.

The difference between regulation controller and this estimation approach is that, the input u is not expected to be too large or too small. However, u is expected to converge to the true value as quick as possible.

LQR method will be used here to design F and see how it affects the estimation trajectory as well as the estimation performance and robustness.

For a given discrete-time system

$$x(k + 1) = Gx(k) + Hu(k) \quad (51)$$

Define cost function J below

$$J = \int_0^{\infty} [x^T(k)Qx(k) + u^T(k)Ru(k)]dk \quad (52)$$

for the state feedback controller

$$u(k) = Fx(k) \quad (53)$$

where Q is an $n \times n$ symmetric positive semidefinite matrix with compatible dimension to x , and R is an $m \times m$ symmetric positive definite matrix with compatible dimension to u .

Let

$$Q = M^T M \quad (54)$$

When (G, H) is stabilizable and (G, M) is detectable, the control

$$u(k) = -R^{-1}H^T Px(k) \quad (55)$$

is an optimal design, where P is the symmetric positive semidefinite solution to the following algebraic Riccati equation (ARE)

$$0 = PG + G^T P + Q - PHR^{-1}HP \quad (56)$$

For the driveline state-space model (21) and (22), choose

$$Q = \begin{bmatrix} 1 & 0 & 0 \\ 0 & 0 & 0 \\ 0 & 0 & 0 \end{bmatrix} = M^T M \quad (57)$$

so that

$$M = [1 \quad 0 \quad 0] \quad (58)$$

and choose

$$R = 100\rho \quad (59)$$

where ρ is a constant used to adjust the poles locations.

For the state model

$$G = \begin{bmatrix} 0.745394 & 0.942042 & -15.957481 \\ 0.000179 & 0.999337 & 0.011227 \\ 0.004369 & -0.016165 & 0.958051 \end{bmatrix} \quad (60)$$

and

$$H = \begin{bmatrix} 0.145693 & -0.000015 \\ 0.000015 & -0.000032 \\ 0.000382 & 0.00000027 \end{bmatrix} \quad (61)$$

the algebraic Riccati equation solution is

$$P = \begin{bmatrix} 2.731796 & 2.138227 \times 10^2 & 1.020960 \\ 2.138227 \times 10^2 & 3.147261 \times 10^5 & -7.110415 \times 10^2 \\ 1.020960 & -7.110415 \times 10^2 & 7.451795 \times 10^3 \end{bmatrix} \quad (62)$$

and the associated control gain is

$$F = [-0.003185 \quad -0.358103 \quad 0.031484] \quad (63)$$

The closed-loop poles are within the unite circle at

$$\begin{aligned} &0.851184347012628 + 0.241746107033041i \\ &0.851184347012628 - 0.241746107033041i \\ &0.999956724568661 + 0.000000000000000i \end{aligned} \quad (64)$$

The corresponding N is

$$N = 3.606914 \quad (65)$$

Note that the 2-norm of control gain is defined and given below.

$$\|F\| = \sqrt{0.003185^2 + 0.358103^2 + 0.031483^2} \quad (66)$$

$$\|F\| = 0.359499 \quad (67)$$

and it is much smaller than the norm of control gain for the deadbeat design

$$\|F_{dead}\| = 9.807029 \times 10^4 \quad (68)$$

The resulting N is also small, leading to much slower response than the deadbeat and conventional pole assignment design. For the given F in (63) and N in (65), the estimated input is shown in the following figure.

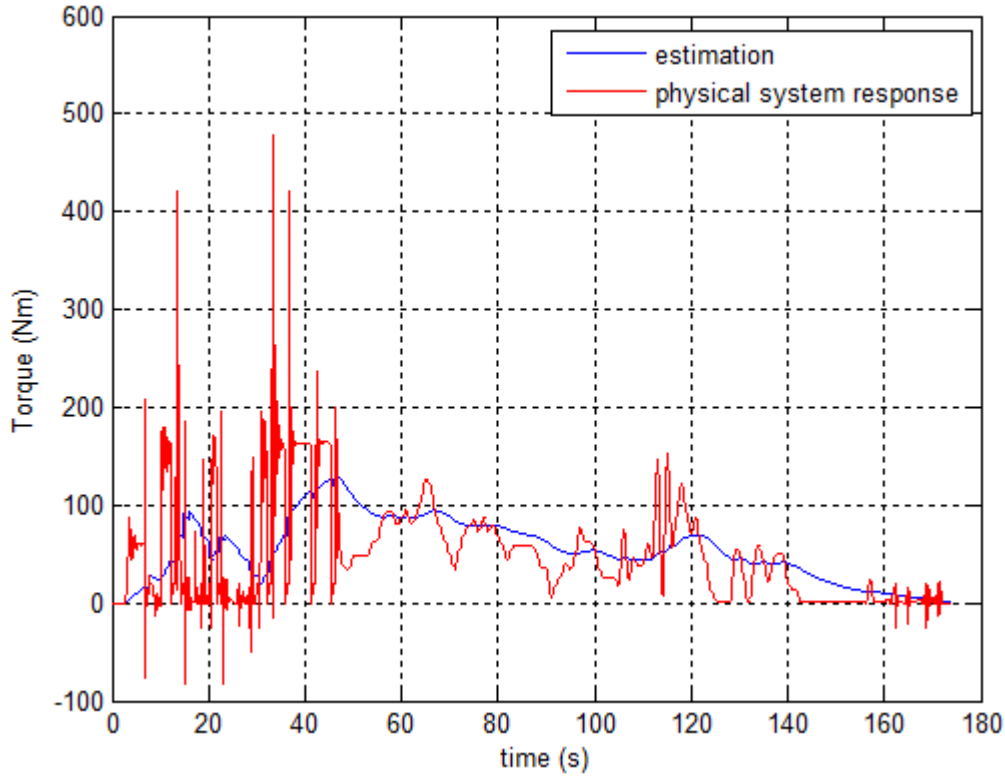


Figure 16. LQR estimated input and actual input torque

The simulation confirms that the system response is slow. For a fast responding system like driveline, the system response time is too slow to predict the actual input.

4.3 Integral Regulation Method (Discrete-Time)

4.3.1 Integral Regulator Design

Another way to regulate the output of state-space model to the desire value is using the integral control. Consider the discrete-time state-space model

$$x(k + 1) = Gx(k) + Hu(k) \quad (69)$$

$$y(k) = Cx(k) \quad (70)$$

Define an extra state z for the error between output and set point

$$z(k + 1) = r(k) - y(k) + z(k) \quad (71)$$

When state z is regulated down to zero, the output converges to the set point. As a result, the augmented system becomes

$$\begin{bmatrix} x(k + 1) \\ z(k + 1) \end{bmatrix} = \begin{bmatrix} G & 0 \\ -C & 1 \end{bmatrix} \begin{bmatrix} x(k) \\ z(k) \end{bmatrix} + \begin{bmatrix} H \\ 0 \end{bmatrix} u(k) + \begin{bmatrix} 0 \\ I \end{bmatrix} r(k) \quad (72)$$

Now, let

$$\tilde{x}(k) = \begin{bmatrix} x(k) \\ z(k) \end{bmatrix}$$

$$\tilde{A} = \begin{bmatrix} G & 0 \\ -C & 1 \end{bmatrix} \quad (73)$$

$$\tilde{B} = \begin{bmatrix} H & 0 \\ 0 & I \end{bmatrix}$$

and

$$\tilde{u}(k) = \begin{bmatrix} u(k) \\ r(k) \end{bmatrix} \quad (74)$$

The system can be expressed as

$$\tilde{x}(k + 1) = \tilde{A}\tilde{x}(k) + \tilde{B}\tilde{u}(k) \quad (75)$$

If a controller

$$\tilde{u}(k) = F\tilde{x}(k) \quad (76)$$

can be designed such that the spectrum radius

$$\rho(\tilde{A} + \tilde{B}F) < 1 \quad (77)$$

the system is stable, and the integrator will steer the output to desire value.

For the driveline system below

$$G = \begin{bmatrix} 0.745394 & 0.942042 & -15.957481 \\ 0.000179 & 0.999337 & 0.011228 \\ 0.004369 & -0.016166 & 0.958052 \end{bmatrix} \quad (78)$$

$$H = \begin{bmatrix} 0.145694 \\ 0.000015 \\ 0.000382 \end{bmatrix} \quad (79)$$

and

$$C = [0 \quad 1 \quad 0] \quad (80)$$

The corresponding matrices \tilde{A} and \tilde{B} are

$$\tilde{A} = \begin{bmatrix} 0.745394 & 0.942042 & -15.957481 & 0 \\ 0.000179 & 0.999337 & 0.011228 & 0 \\ 0.004369 & -0.016166 & 0.958052 & 0 \\ 0 & -1 & 0 & 1 \end{bmatrix} \quad (81)$$

$$\tilde{B} = \begin{bmatrix} 0.145693 & 0 \\ 0.000015 & 0 \\ 0.000382 & 0 \\ 0 & 1 \end{bmatrix} \quad (82)$$

Now the system has two inputs and one output again, and the input cannot be estimated.

However, the set point of discrete-time state-space model is available. Hence, the \tilde{B} can be reduced down to

$$\tilde{B} = \begin{bmatrix} 0.145693 \\ 0.000015 \\ 0.000382 \\ 0 \end{bmatrix} \quad (83)$$

Now, using pole placement method to place poles of $\tilde{A} + \tilde{B}F$ at ± 0.1 and ± 0.2 , the associated control gain F is

$$F = \begin{bmatrix} -10.728322 \\ -4.193968 \times 10^4 \\ -3.982761 \times 10^3 \\ 1.008024 \times 10^5 \end{bmatrix}^T \quad (84)$$

The estimation system architecture is shown below

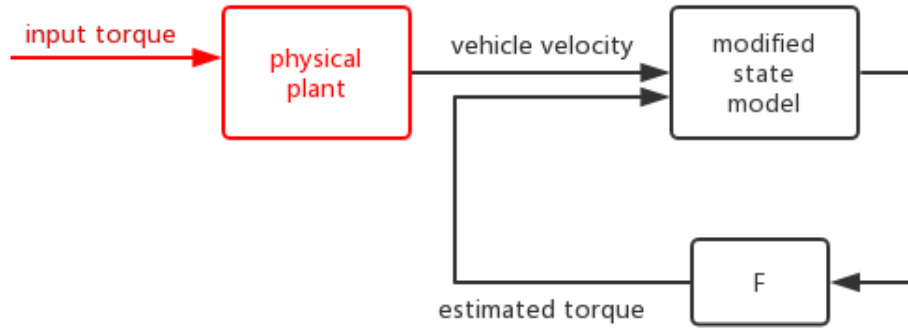


Figure 17. Block diagram of integral control estimation

Similar to before, since the state feedback requires all four states, the system matrix C is modified to identity as below

$$C = \begin{bmatrix} 1 & 0 & 0 & 0 \\ 0 & 1 & 0 & 0 \\ 0 & 0 & 1 & 0 \\ 0 & 0 & 0 & 1 \end{bmatrix} \quad (85)$$

to make all states available. The simulated system outputs of the state-space model converge to these of the physical model as shown in Figure 18.

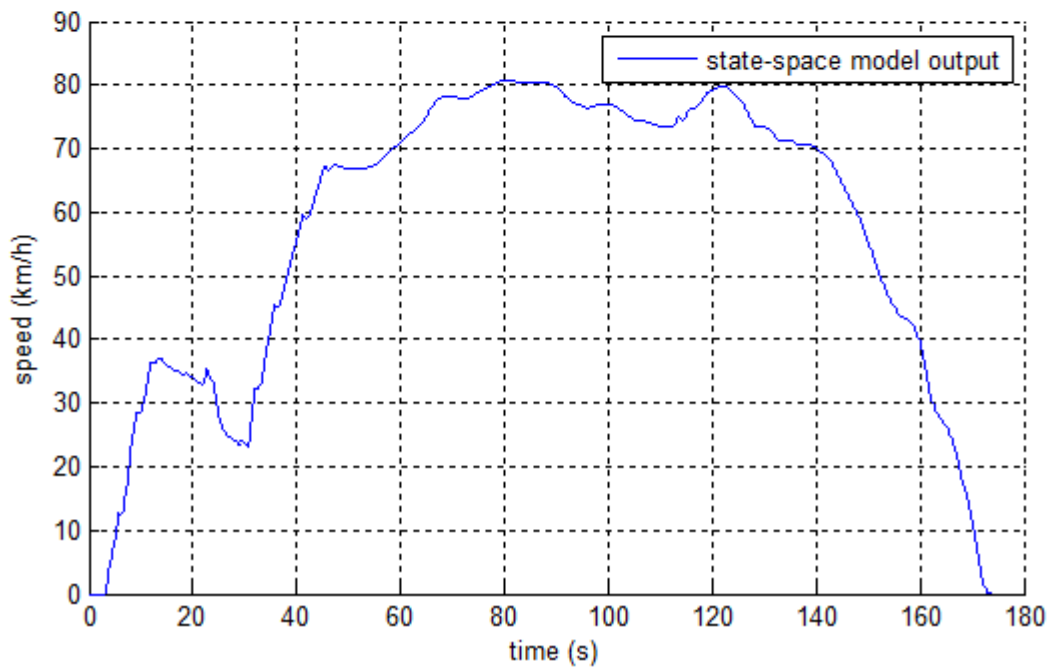
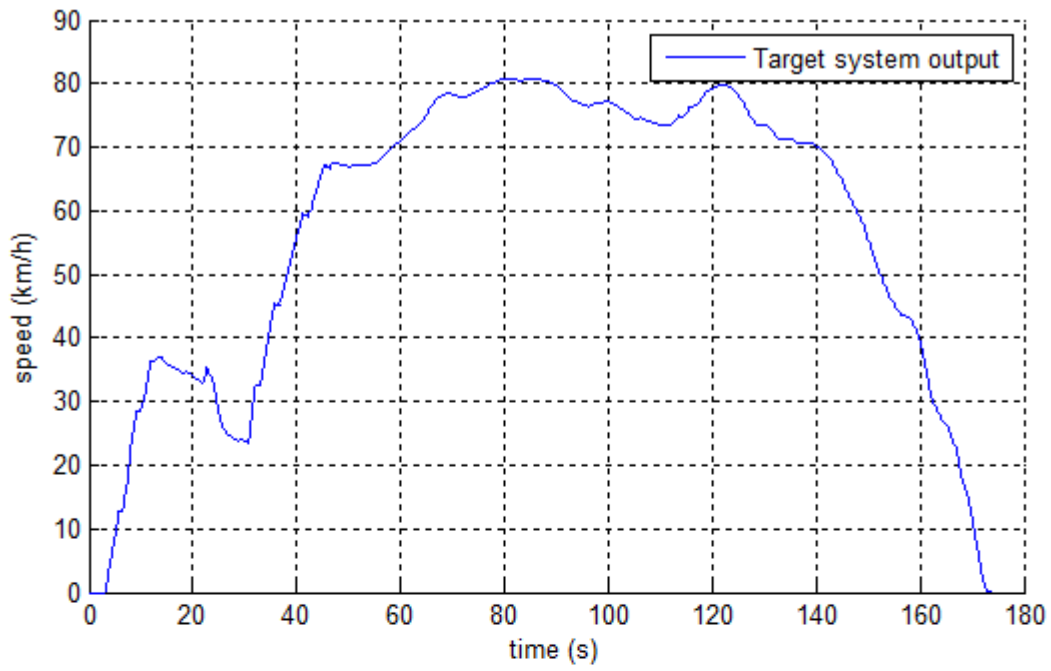


Figure 18. Target system output (top) and state-space model output (bottom)

However, each time the clutch engages and dis-engage, there exists very large overshoot with relatively slow response time, compared with the feedforward control.

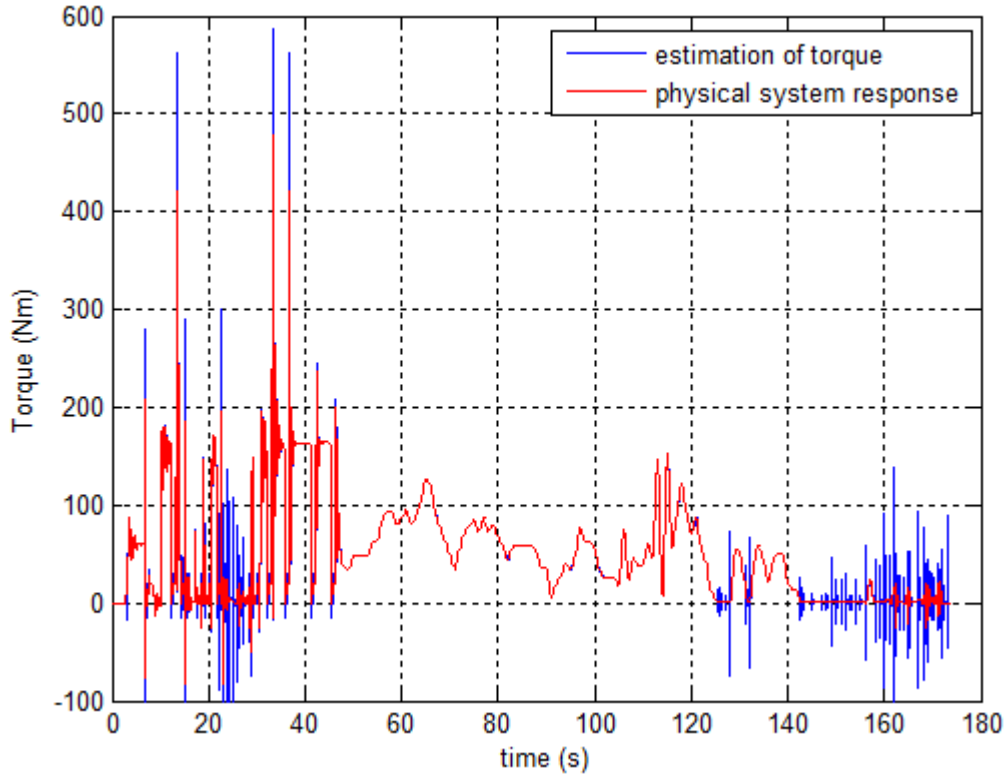


Figure 19. Integral control failed to track the physical system input when clutch state changes with closed-loop poles at ± 0.1 and ± 0.2

4.3.2 Deadbeat Design Comparison

Next, different pole locations are placed to see if the overshoot and response time can be reduced. Using the pole place command, the gain

$$F_1 = \begin{bmatrix} -11.936269 \\ -1.298288 \times 10^5 \\ -1.253874 \times 10^2 \\ 2.863704 \times 10^4 \end{bmatrix}^T \quad (86)$$

assigns the poles to

$$\begin{bmatrix} 0.5 \\ -0.5 \\ 0.8 \\ -0.8 \end{bmatrix}^T \quad (87)$$

with the following estimation result.

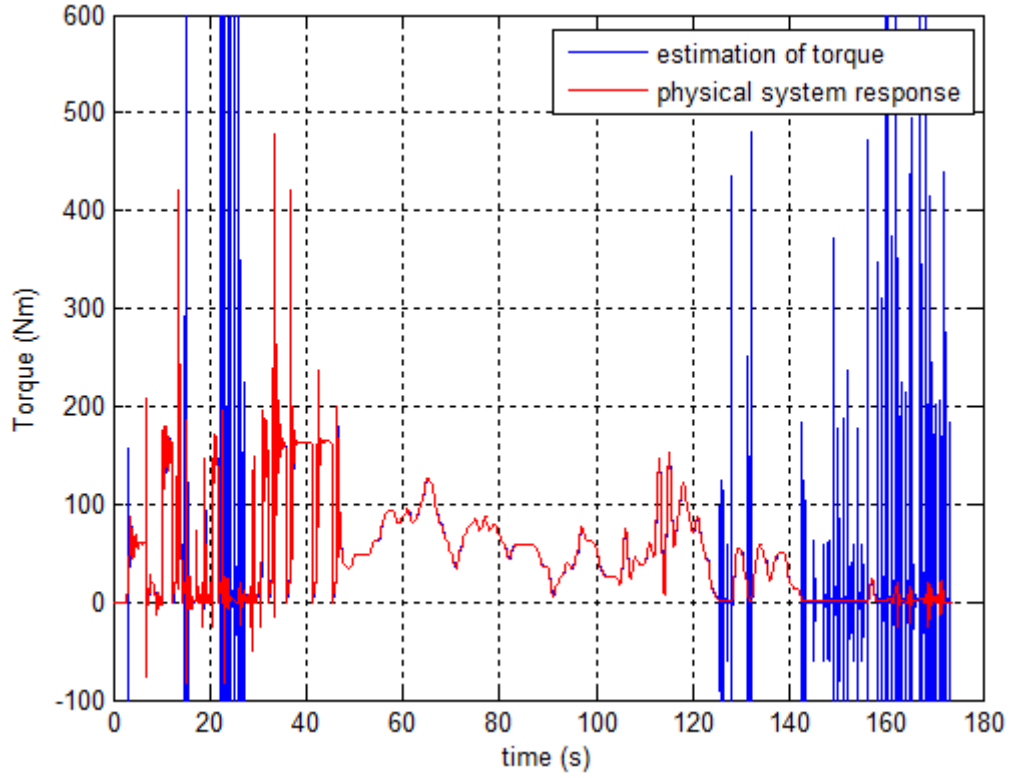


Figure 20. Estimation results for closed-loop poles at ± 0.5 and ± 0.8

With poles are assigned at ± 0.5 and ± 0.8 , the overshoot is increased significantly. From the pole location characteristics for discrete-time systems, assigning poles far away from the origin increases the system response time.

Now, try to design two control gains with closed-loop poles closer to the origin: F_2 at $\pm 0.01, \pm 0.02$ and F_3 at $\pm 0.001, \pm 0.002$, where F_2 and F_3 are given below

$$F_2 = \begin{bmatrix} -10.6269 \\ -3.323911 \times 10^4 \\ -4.357692 \times 10^3 \\ 1.0601 \times 10^5 \end{bmatrix}^T \quad (88)$$

$$F_3 = \begin{bmatrix} -10.6258 \\ -3.322505 \times 10^4 \\ -4.355979 \times 10^3 \\ 1.059541 \times 10^5 \end{bmatrix}^T \quad (89)$$

The simulated estimation results are given in the two figures below.

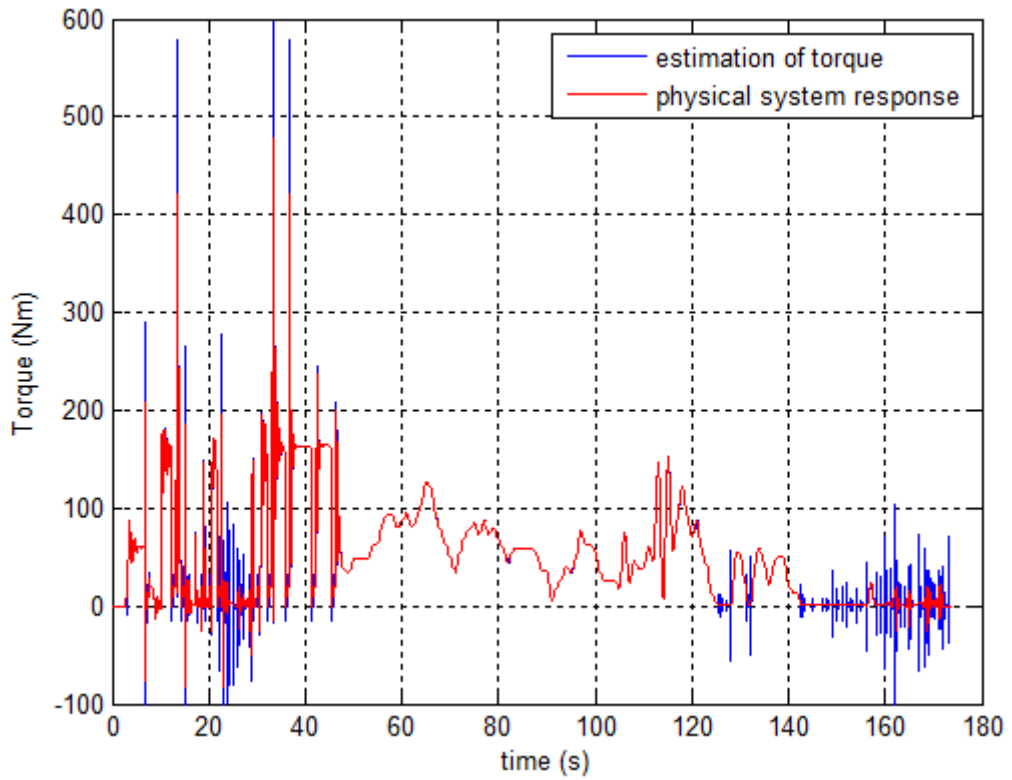


Figure 21. Integral control of poles assigned at ± 0.01 and ± 0.02

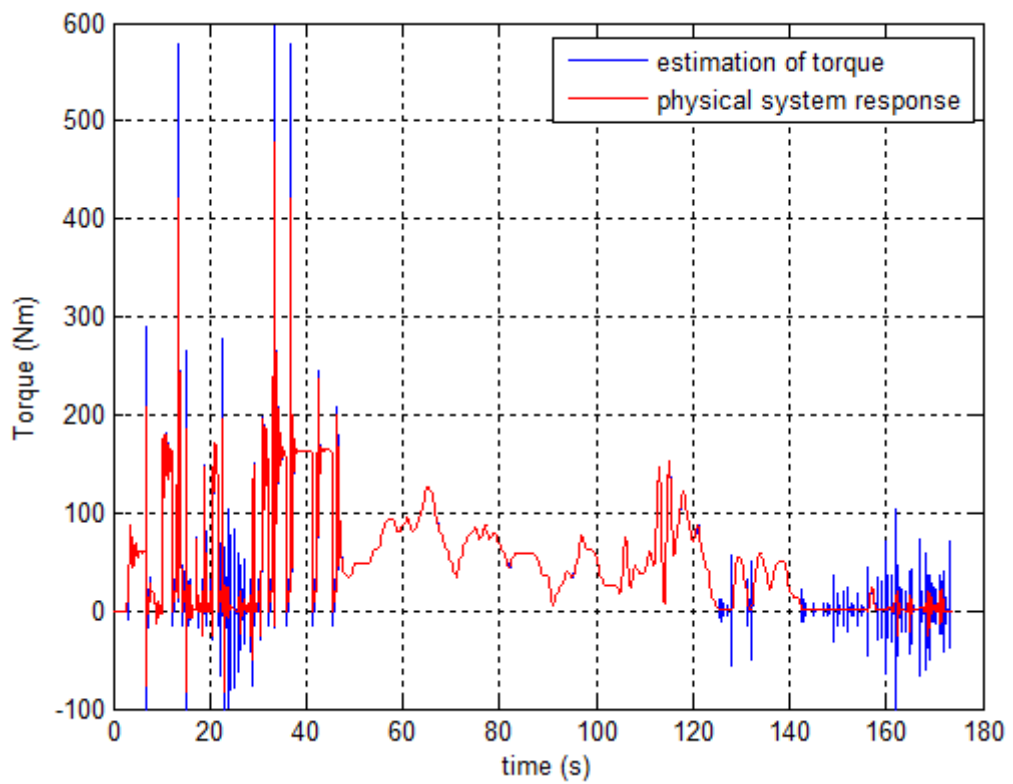


Figure 22. Integral control of poles assigned at ± 0.001 and ± 0.002

As the assigned poles gets close to the origin, the estimation performance of the integral

design gets close to that of dead-beat design. But there is not much improvement to the overshoot performance when the assigned poles are moved from $\pm 0.01, \pm 0.02$ to $\pm 0.001, \pm 0.002$ since they are already very closed to the origin and the associated controllers are basically deadbeat controllers.

Each time the clutch engages and disengages, there exists very large estimation error. Although the closed-loop system is stable, it still takes more time steps to converge to the desired value than that for the feedforward regulator. Overshoot is another problem (see Figure 21 and Figure 22).

The advantage of the integral regulator is its tracking accuracy when the system is at steady-state without disturbance. A comparison of integral and feed forward regulators is shown in Figure 23. Between 58 and 58.4 second, without transient disturbance (slow input torque changes), the estimation error of the feed forward regulator is small, especially at 58.3 second mark, and however, the estimation error of the integral regulator is accurate over the entire time.

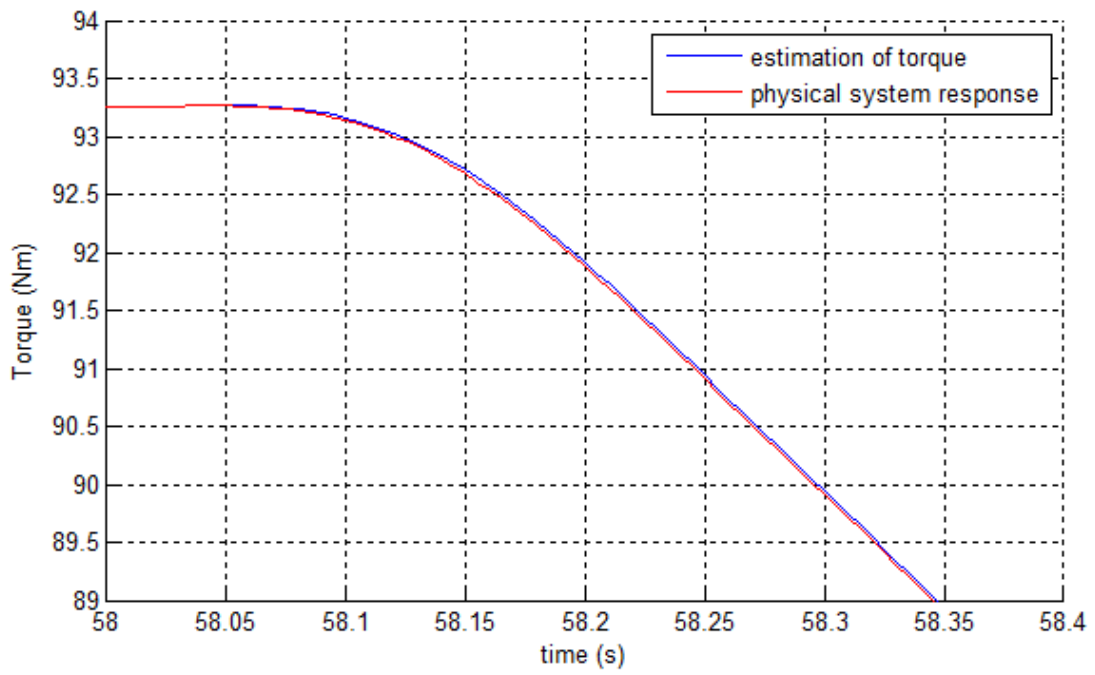
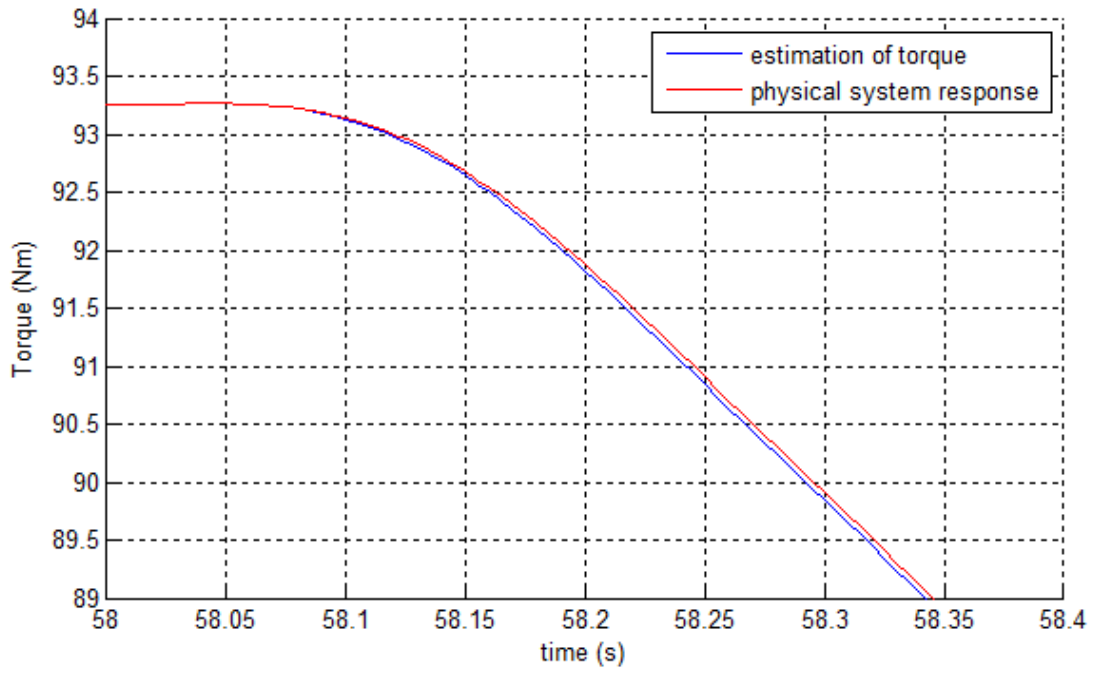


Figure 23. Feedforward regulator (top) compare with integral regulator (bottom) between 66 and 66.2 second

CHAPTER 5: EFFECTS OF MODELING ERROR AND SOLUTIONS

5.1 Introduction

In real life, the total vehicle mass varies, depending on the vehicle load. In this Chapter, a case study will be conducted when vehicle mass changes. The robustness of the state-space model will be investigated, and a solution will be provided if the model is not robust to the vehicle mass change.

5.2 Modeling Error Due to Change of Vehicle Mass

In the current model, the total vehicle mass is 1600 kg. The estimated torque is very precise since the state model is derived based on this mass. It is interesting to know how well this model can predict the torque when the mass deviates away from 1600 kg.

In this case, assume that the vehicle mass is increased by 500 kg so that the total vehicle mass is now 2100 kg. Using the state-space model for vehicle mass of 1600 kg, the clutch output torque estimated is shown in the figure below [16].

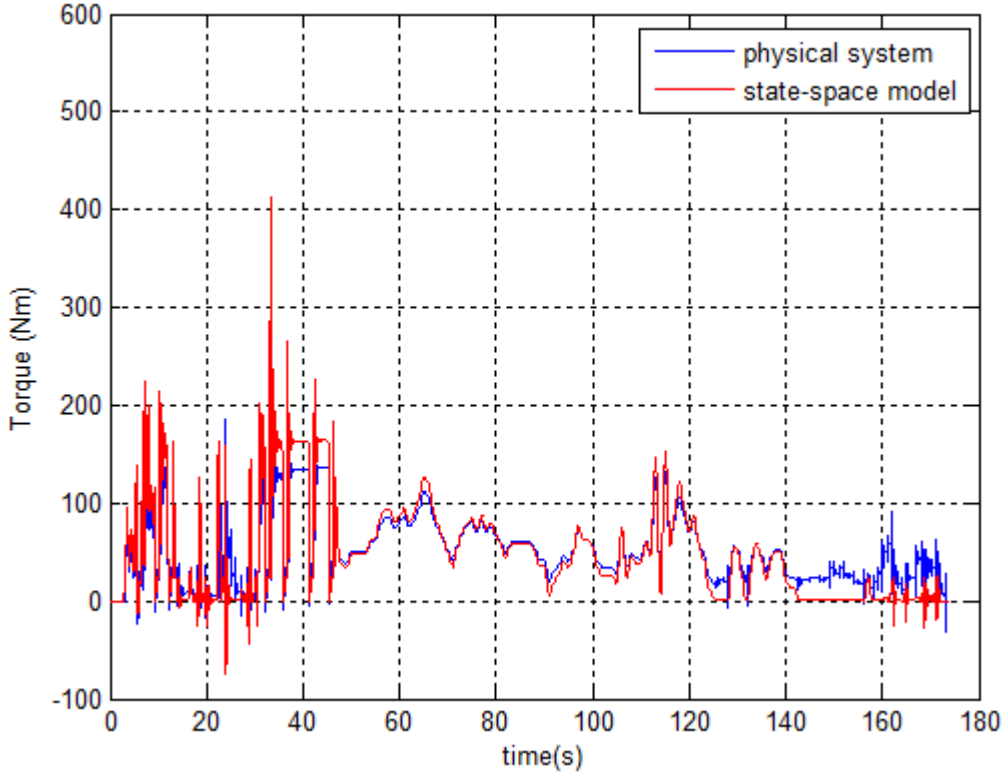


Figure 24. Estimation of torque when modeling error exists

It shows that when vehicle mass modeling error exists, the system is not able to predict torque precisely.

5.3 Solutions to Handle the Vehicle Mass Modeling Error

The solution to reduce the vehicle mass modeling error is to estimate the vehicle mass on-line and modify the state-space model used for estimation. When the clutch is fully engaged, the engine shaft is solidly connected to wheels and the torque transmitted by the clutch is known. Since the vehicle motion is dominated by

$$J_t \times \ddot{\theta} = T_{in}(GR \times final\ ratio \times \dot{v}) + T_{loss} \quad (90)$$

where J_t is total inertia calculated from vehicle mass and wheel inertia J_w

$$J_t = 4 \times J_w + R^2 M \quad (91)$$

\dot{v} is vehicle acceleration that can be found by taking derivative of the measured velocity, and

T_{loss} is defined earlier as below

$$T_{loss} = \frac{1.225}{2} C_d A v^2 + M \mu_{ground} g + T_{brake} \quad (92)$$

By manipulating above formula, the mass of vehicle can be estimated using the following equation

$$M = \frac{(3.7 \times GR) T_{in} - \frac{1.225}{2} C_d A v^2 - 4 J_w \dot{v} - T_{brake}}{R^2 \dot{v} + \mu_{ground} g} \quad (93)$$

With the updated mass, the state-space model can be updated to be used next.

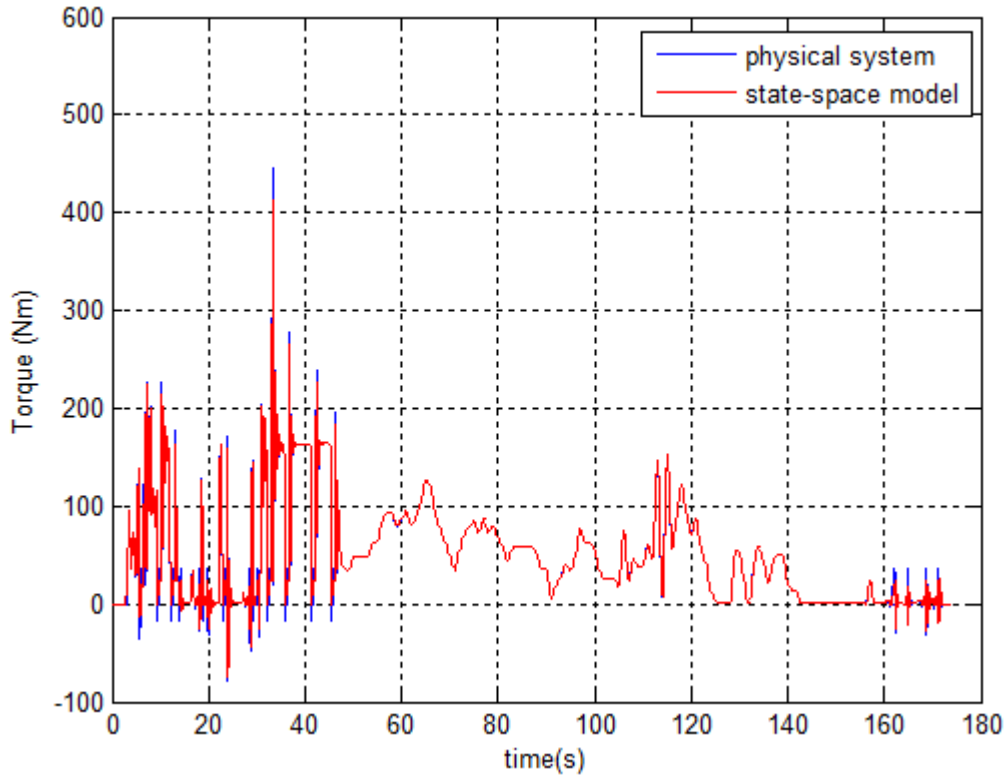


Figure 25. Torque estimation with real-time estimated vehicle mass

5.4 Gradient Effect

From the previous chapter it is known

$$T_{gradient} = Mass \times \sin\theta \times g \times R \quad (94)$$

and

$$T_{loss} = T_{brake} + T_{Road} + T_{wind} + T_{gradient} \quad (95)$$

If road gradient exists, the vehicle mass M can be alternatively calculated with following formula

$$M = \frac{(3.7 \times GR)T_{in} - \frac{1.225}{2}CdAv^2 - 4J_w\dot{v} - T_{brake} - T_{gradient}}{R^2\dot{v} + \mu_{ground}g} \quad (96)$$

assuming that a road gradient sensor is available on vehicle for measuring θ so that $T_{gradient}$ is known.

CHAPTER 6: FRICTION COEFFICIENT CALCULATION

6.1 Calculation Method and Result

The friction coefficient is calculated using the clutch output and measured pressure between both clutch surfaces. In the previous section, the clutch output torque is estimated by various methods. The pressure between both clutch plates is assumed to be measurable. Note that many vehicles do have clutch pressure sensors on board.

The kinetic friction coefficient can be calculated by the following formula

$$\mu_k = \left| \frac{T}{PArN} \right| \quad (97)$$

where T is the torque transmitted through the clutch, P is pressure between clutch surfaces, A is clutch effective area, r is clutch effective radius and N is number of clutch plate pairs.

Since kinetic friction coefficient only occurs during slipping, a detection algorithm will be designed to only calculate friction coefficient during slipping.

When velocity of each side of clutches is mismatched and pressure between clutches is not zero, the clutch is under slipping. At the start of slipping, there exists torque estimation error, and the estimation error will diminish within about seven time steps for the feedforward estimation with the deadbeat design.

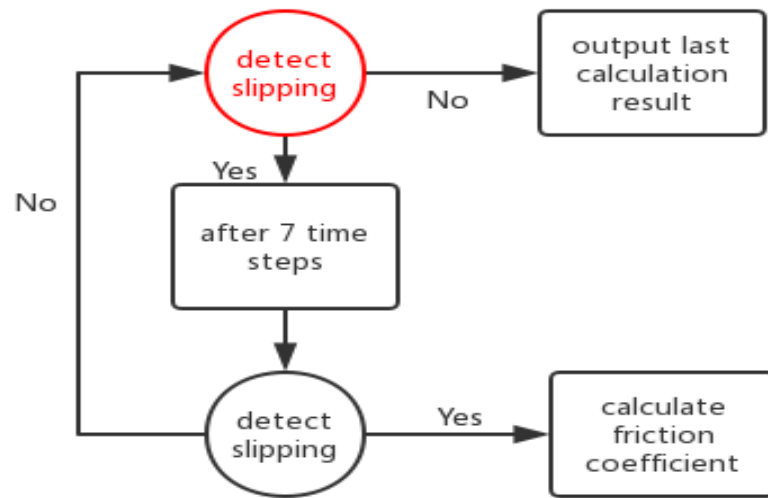


Figure 26. Detection algorithm flowchart

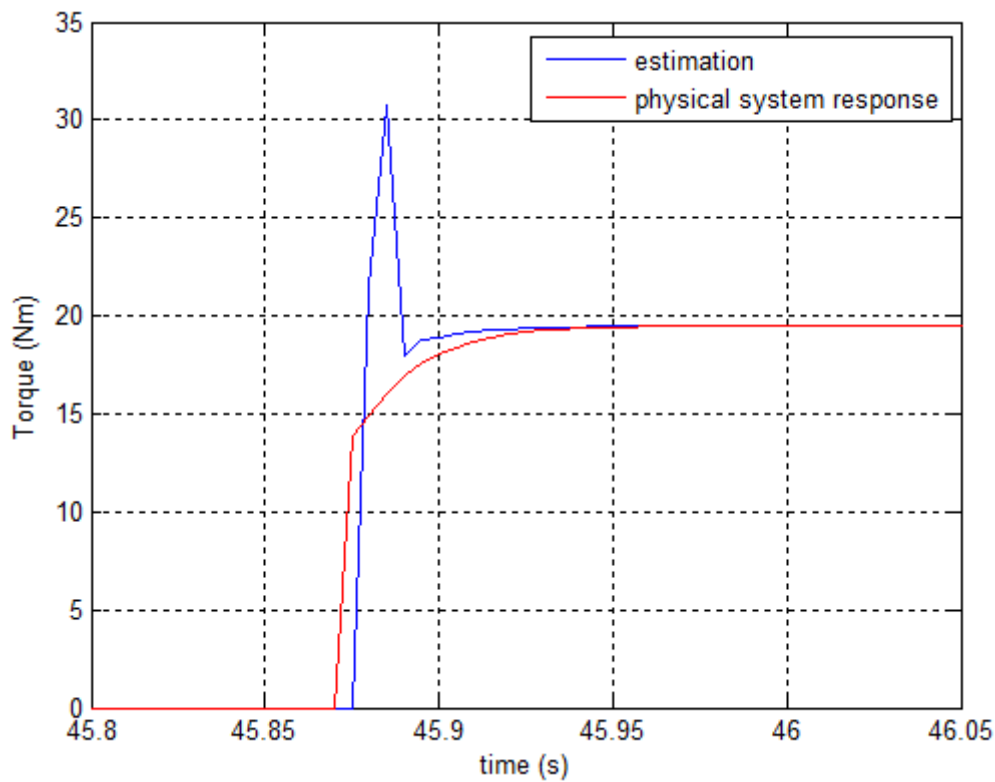


Figure 27. Error diminish within few time steps during slipping

After slipping occurs, the detection algorithm will wait for seven time steps (until the torque estimation converges) to start detection. If clutch is slipping after seven time steps, the μ_k will be updated. Whenever the clutch is not slipping, the detection algorithm keeps

estimated μ_k unchanged.

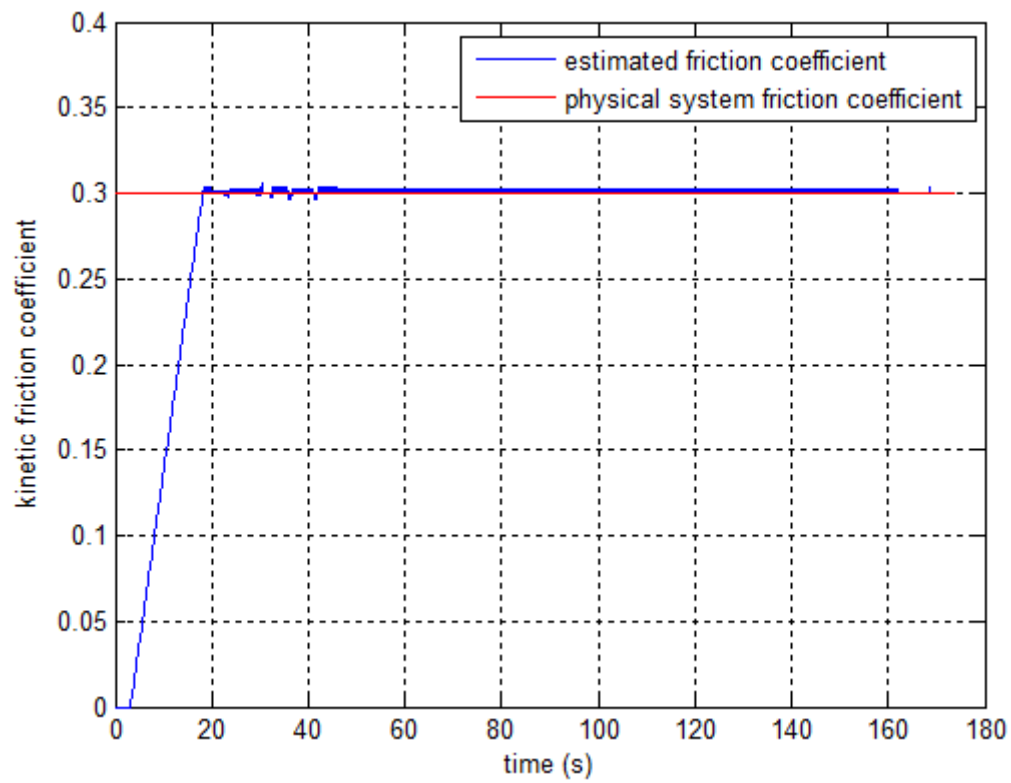


Figure 28. Estimated friction coefficient

As shown in Figure 28, the estimated friction coefficient is about 0.3 and it is very close to the true value.

CHAPTER 7: CONCLUSION AND FUTURE WORK

7.1 Conclusion

Before the simulation, the clutch kinetic friction coefficient in the physical model is set to 0.3 and the simulated estimation results show that the estimation is very accurate. The main idea of this thesis is transforming the entire vehicle drive-line system into a linear state-space model and estimate the input torque based on the system output (vehicle speed).

The estimation method developed in this thesis can be used for other physical systems with system input to be estimated. In this thesis, two main regulation methods are used, integral and feedforward. Feedforward regulation works very well for estimating the system input since it converges to the actual value very faster (within seven time steps) with small overshoot. However, for the system with slow dynamics, integral regulation can be able to reduce the estimation error at steady state.

7.2 Future Improvement

The driveline model can be improved using more springs and dampers to replace the rigid shaft and to increase system degree of freedoms. Currently there are only two degrees of freedoms. Vehicle tire slipping loss can also be model with MAGIC tire formula. The estimation method can be further tested with other regulation and tracking methods. The state-space model used in simulation studies is linear, a nonlinear model could be used in the future to improve the estimation performance.

APPENDIX

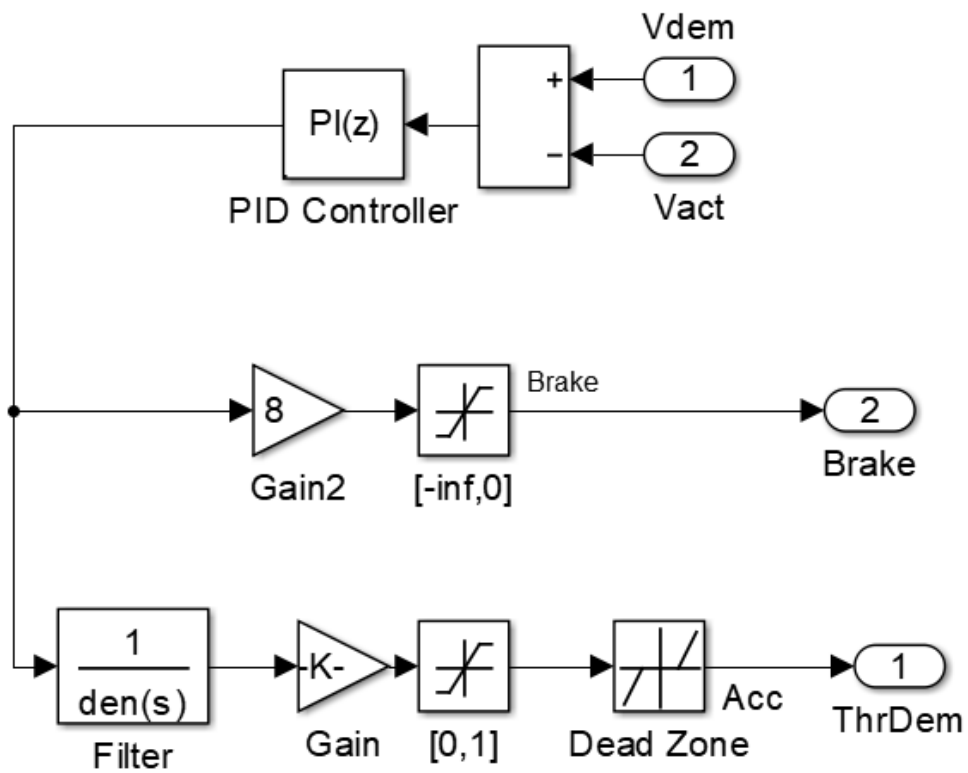


Figure 29. Driver model for acceleration and brake pedal inputs

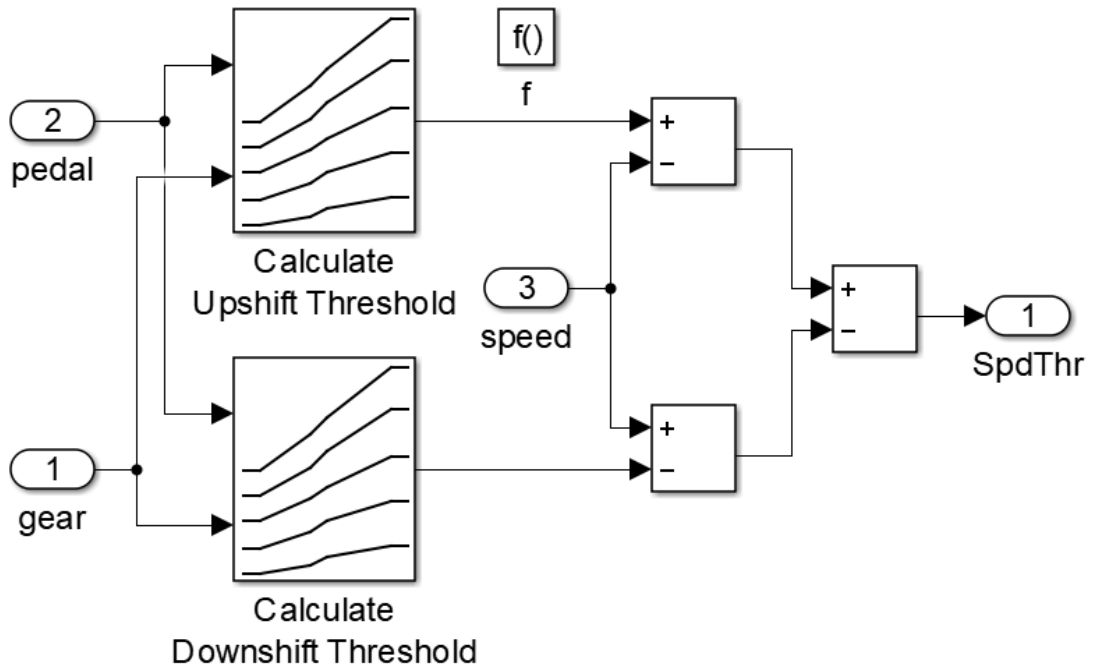


Figure 30. Shifting threshold determination

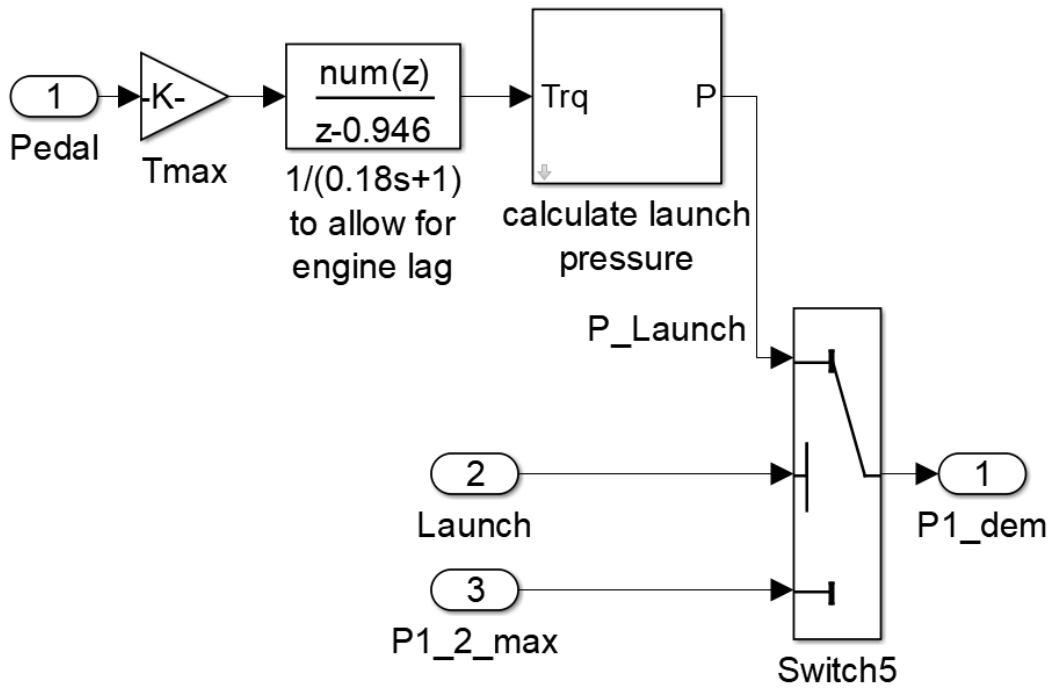


Figure 31. Switch between start-up and driving modes and associated pressure

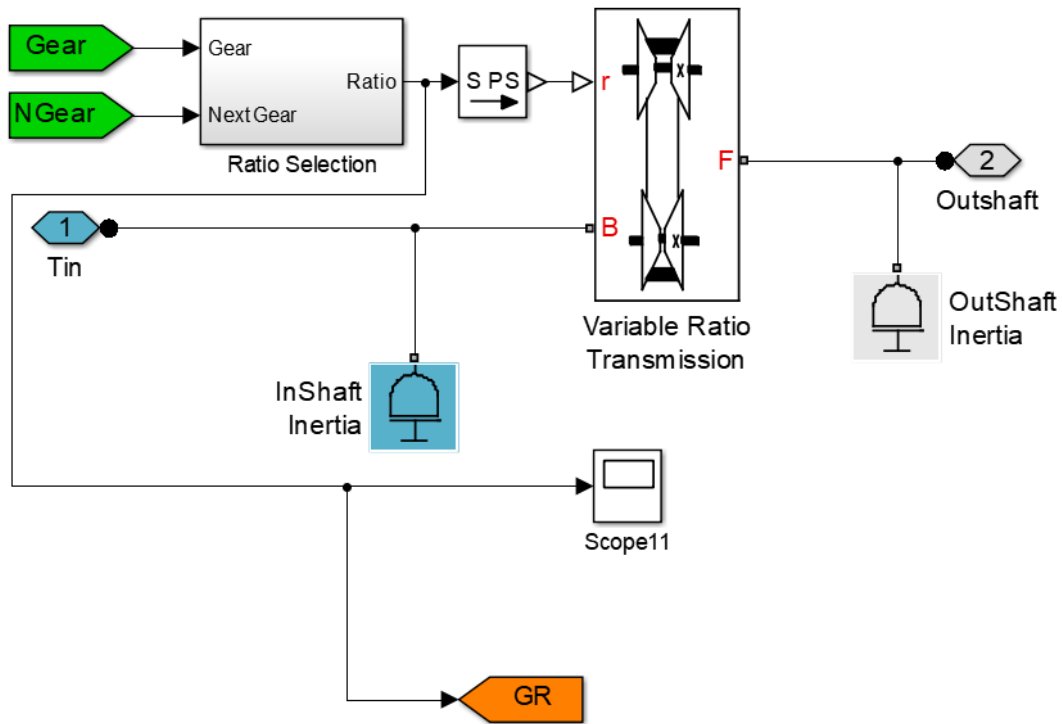


Figure 32. The Simulink gear-box model

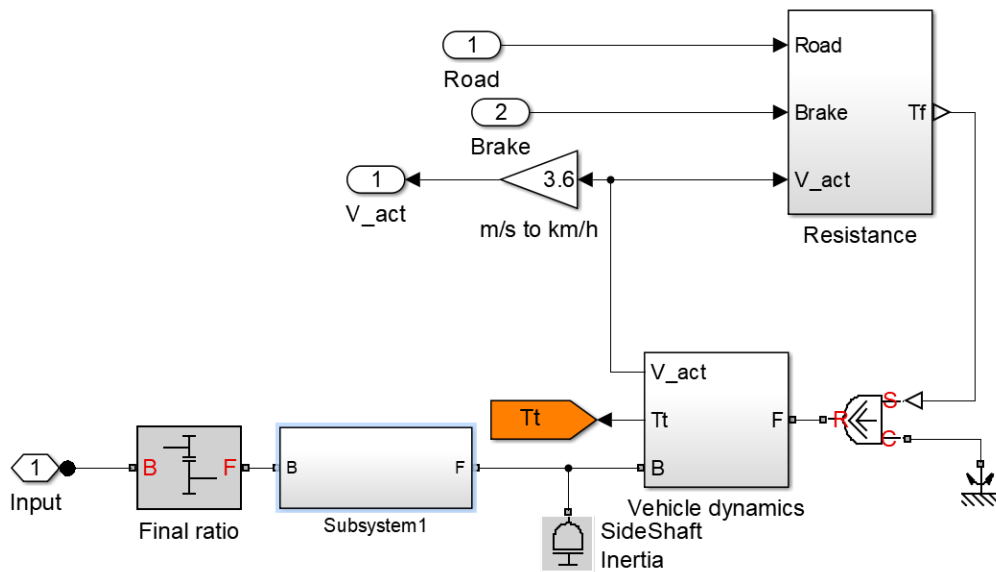


Figure 33. Simulink driveline diagram without transmission

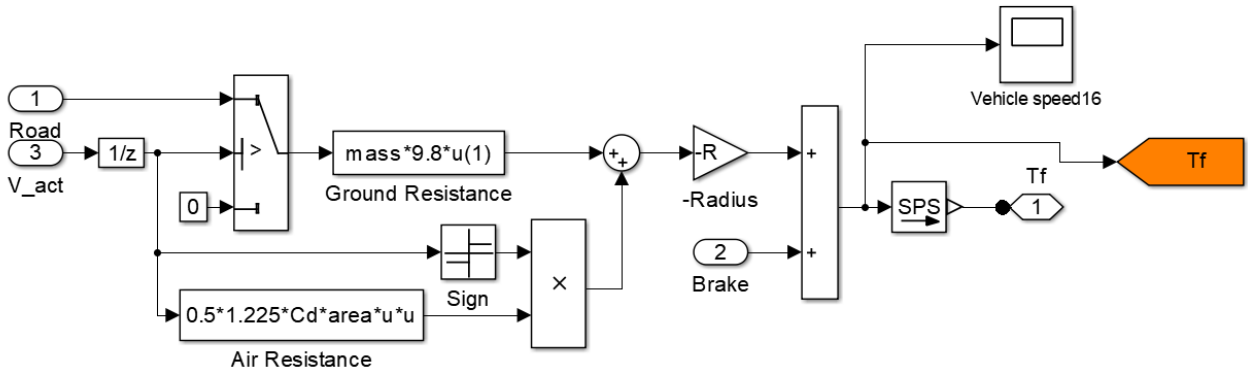


Figure 34. Torque loss calculation

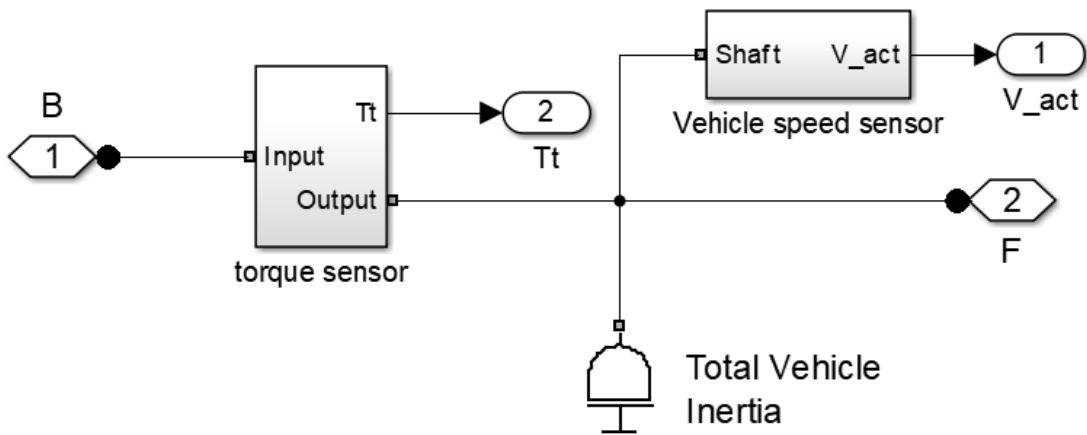


Figure 35. Vehicle dynamic responses

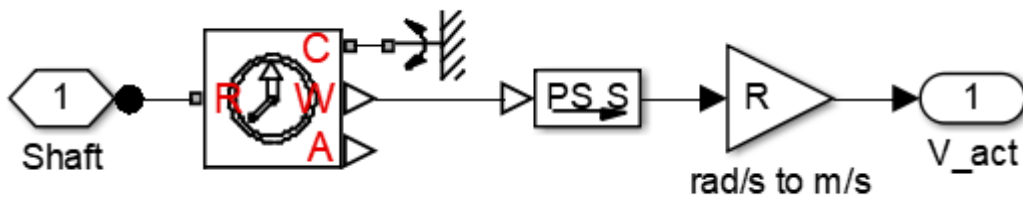


Figure 36. Vehicle speed sensor.

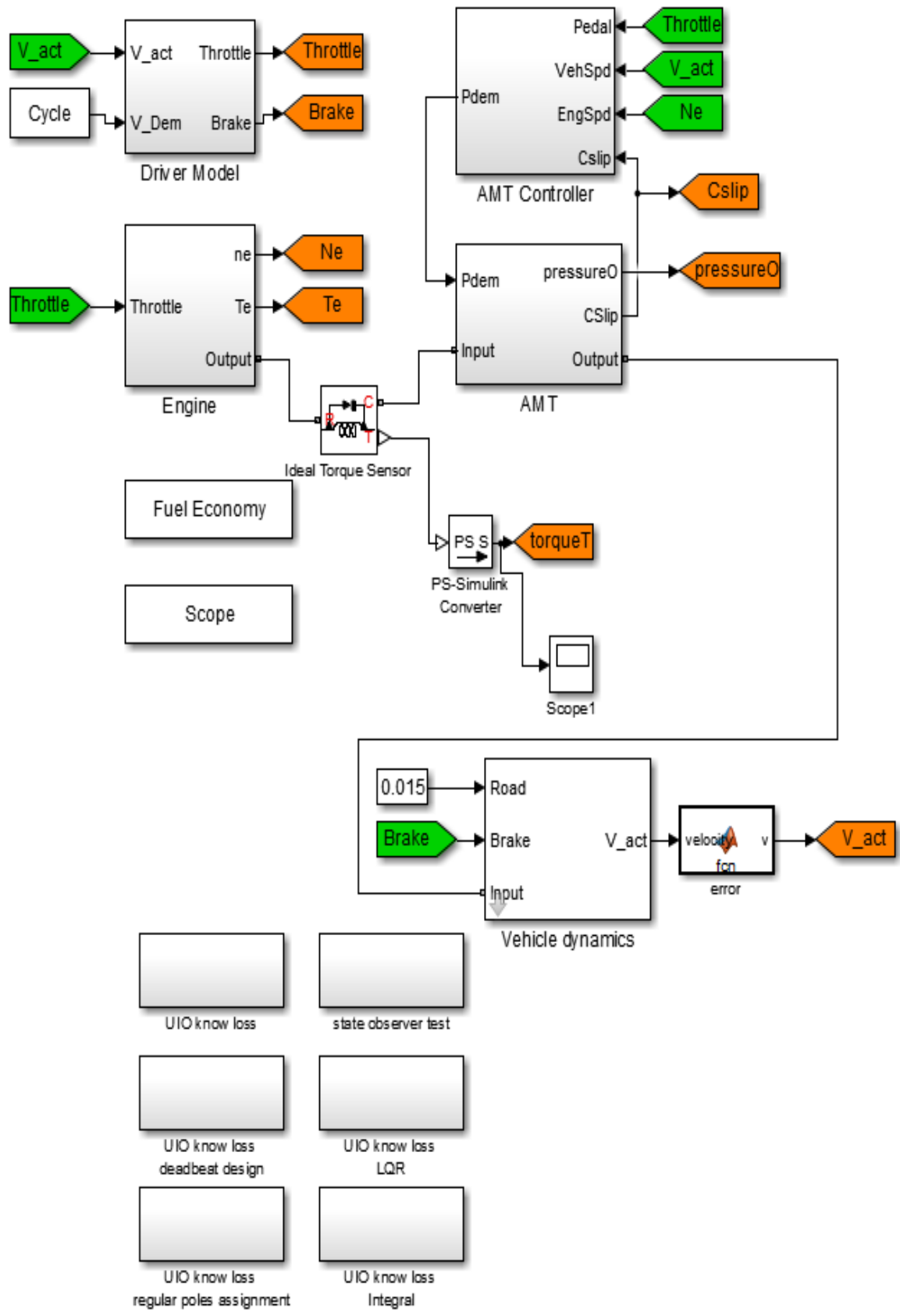


Figure 37. Simulink system model overview

REFERENCES

REFERENCES

- [1] Glielmo, Luigi & Iannelli, Luigi & Vacca, Vladimiro & Vasca, Francesco. (2006). Gearshift control for automated manual transmissions. *Mechatronics*, IEEE/ASME Transactions on. 11. 17 - 26. 10.1109/TMECH.2005.863369.
- [2] Chengsheng Miao, Haiou Liu, Guoming G Zhu: “Three-parameter transmission gear shifting schedule for improved fuel economy”, *Proceedings of the Institution of Mechanical Engineers, Part D: Journal of Automobile Engineering*. Vol 232, Issue 4, pp. 521 – 533.
- [3] L. Glielmo, L. Iannelli, V. Vacca, and F. Vasca, “Speed control for auto-mated manual transmission with dry clutch,” in Proc. 43th IEEE Conf. Decision and Control, Atlantis, Bahamas, 2004, pp. 1709–1714.
- [4] J. Slicker and R. N. K. Loh, “Design of robust vehicle launch control system,” *IEEE Trans. Contr. Syst. Technol.*, vol. 4, no. 4, pp. 326–335, Jul.1996.
- [5] Donghao Hao, Changlu Zhao, and Ying Huang, “*A Reduced-Order Model for Active Suppression Control of Vehicle Longitudinal Low-Frequency Vibration*,” *Shock and Vibration*, vol. 2018, Article ID 5731347, 22 pages, 2018.
- [6] J. S. Bang, Y.-K. Ko, and T.-H. Jung, “*The Active Damping Control to Reduce Driveline Oscillations for Electric Vehicles Using Wheel Speeds*,” *SAE Technical Papers*, vol. 2015-, no. April, 2015.
- [7] M. Bartram, G. Mavros, and S. Biggs, “*A study on the effect of road friction on driveline vibrations*,” *Proceedings of the Institution of Mechanical Engineers, Part K: Journal of Multibody Dynamics*, vol. 224, no. 4, pp. 321–340, 2010.
- [8] L. Jin and O. Minggao, “*A Study on Surge Control Strategy for Diesel Powertrain*,” *Automotive Engineering*, vol. 28, pp. 238– 241, 2006.
- [9] X. Lu, H. Chen, H. Zhang, P. Wang, and B. Gao, “*Design of model predictive controller for anti-jerk during tip-in/out process of vehicles*,” in *Proceedings of the 30th Chinese Control Conference, CCC 2011*, pp. 3395–3400, chn, July 2011.
- [10] R.A. DeCarlo, *Linear Systems*, Prentice Hall, Englewood Cliffs, NJ, 1989.
- [11] Y. Lei, M. Niu, and A. Ge, “*A research on starting control strategy of vehicle with AMT*,” in Proc. FISITA World Automotive Congress, Seoul, Korea, 2000.
- [12] P.J. Antsaklis and A.N. Michel, *Linear Systems*, Birkh“auser, Boston, MA, 2006.
- [13] P.Hr. Petkov, N.D. Christov, and M.M. Konstantinov, *Computational Methods for Linear Control Systems*, Prentice Hall-International Series, Englewood Cliffs, NJ, 1991.
- [14] R.V. Patel, A.J. Laub, and P.M. VanDooren, Eds., *Numerical Linear Algebra Techniques*

for Systems and Control, IEEE Press, Piscataway, NJ, 1993.

- [15] J. Fredriksson and B. Egardt, “*Nonlinear control applied to gearshifting in automated manual transmission*,” in Proc. 39th IEEE Conf. Decision and Control, Sydney, Australia, 2000, pp. 444–449.
- [16] Sorniotti, “*Driveline modeling, experimental validation and evaluation of the influence of the different parameters on the overall system dynamics*,” SAE Technical Papers, 2008.